INFORMATION TO USERS

This manuscript has been reproduced from the microfilm master. UMI films the text directly from the original or copy submitted. Thus, some thesis and dissertation copies are in typewriter face, while others may be from any type of computer printer.

The quality of this reproduction is dependent upon the quality of the copy submitted. Broken or indistinct print, colored or poor quality illustrations and photographs, print bleedthrough, substandard margins, and improper alignment can adversely affect reproduction.

In the unlikely event that the author did not send UMI a complete manuscript and there are missing pages, these will be noted. Also, if unauthorized copyright material had to be removed, a note will indicate the deletion.

Oversize materials (e.g., maps, drawings, charts) are reproduced by sectioning the original, beginning at the upper left-hand corner and continuing from left to right in equal sections with small overlaps. Each original is also photographed in one exposure and is included in reduced form at the back of the book.

Photographs included in the original manuscript have been reproduced xerographically in this copy. Higher quality 6" x 9" black and white photographic prints are available for any photographs or illustrations appearing in this copy for an additional charge. Contact UMI directly to order.

UMI

The chess board is the world; the pieces are the phenomena of the universe; the rules of the game are what we call the laws of Nature. The player on the other side is hidden from us. We know that his play is always fair, just, and patient. But also we know, to our cost, that he never overlooks a mistake, or makes the smallest allowance for ignorance.

T.H. HUXLEY

Where observation is concerned, chance favours only the prepared mind.

LOUIS PASTEUR

-

University of Alberta

The Effect of Finely Divided Water on

Premixed Laminar Flames

by

MIKAEL FREDRIK KNUTAR ©

A thesis submitted to the Faculty of Graduate Studies and Research in partial

fulfillment of the requirements for the degree of Master of Science

Department of Mechanical Engineering

Edmonton, Alberta

Spring 1998

University of Alberta

Faculty of Graduate Studies and Research

The undersigned certify that they have read, and recommend to the Faculty of Graduate Studies and Research for acceptance, a thesis entitled The Effect of Finely Divided Water on Premixed Laminar Flames submitted by Mikael Fredrik Knutar in partial fulfillment of the requirements for the degree of Master of Science.

Dr. C-Q Ru

Dr. J. McMullin

Dr. L.W. Kostiuk

Dr. W.H. Finlay

April 3, 1998

ABSTRACT

A study of flame behaviour with water droplets introduced into the reactants of premixed flames has been investigated. The flame configuration studied was a burner stabilized, conical, laminar, methane and air flame. The equivalence ratio was varied from 0.78 to 1.4. The water droplet concentration was varied from 0.088 percent to 1.2 percent by reactant mass fraction.

It was found that reactant dilution is an important effect in decreasing the flame speed initially. As the water droplet concentration increases, the dominant effect on flame propagation is cooling of the flame. A simple computational model indicates that droplets should be less than 5 micrometers in size for optimal reduction of flame speed.

A novel method for producing fine sprays was also investigated. Water was introduced into liquid carbon dioxide under high pressure. The mixture was expanded through a small nozzle resulting in a dense spray with a mass median diameter of 4.5 micrometers.

ACKNOWLEDGEMENTS

I wish to thank the following people for their support in making this thesis a success.

Dr. Larry Kostiuk, for your brilliant insight, ideas, and friendship

Dr. Warren Finlay, for your support, creative thinking, and friendship

Dr. Roger Toogood, for your invaluable insight into the fascinating world of numerical methods.

Dr. D. Steigmann, whose homework problems in continuum mechanics made me expand my brain capacity by 20 percent

Mr. Alan Muir, Mr. Tony vanStraten, Mr. Max Schubert, without whose help none of my mechanical designs would have gotten further than the drawing board.

TABLE OF CONTENTS

LIST OF TABLES

LIST OF FIGURES

1. INTRODUCTION

Until recently, Halon 1301 (trifluoromonobromomethane) has been the primary choice for flame suppression agents. Halon 1301 is an excellent fire suppression medium. Roughly 15 to 20 percent Halon 1301 by volume will suppress explosions. Combustion inception is prevented at a volume concentration of five percent. A Halon fire suppression system operates by interrupting the chemical reactions in the flame zone. The pool of radicals available for the combustion process is depleted by allowing Halon to react with free radicals in the flame. As the concentration of radicals in the flame approaches zero, a rapid suppression of the combustion process is accomplished.

Unfortunately, Halon 1301 is a health hazard. Inhaling the gas can cause heart irregularities, unconsciousness, and death, although occasional exposure to Halon 1301 is considered "safe".

There is also an environmental concern regarding extensive use of Halon 1301 since it depletes the ozone layer. Effective January 1, 1994, the production and importation of new Halon was banned, and the search for a safe replacement began.

One viable technology for fire suppression is fine water mists. Water is one of the most common substances on earth, and water vapour is non-toxic when inhaled. Water is also commonly available, and is inexpensive. However, Halon has a significant advantage over water mist, since Halon is easier to disperse, and a

water mist system would require considerable engineering design to be effective. In addition, spraying water in electrical installations could damage equipment, while Halon gas does not. Despite these difficulties, fine water mists have been applied in many engineering applications. The two most prominent applications so far have been the extinguishment of liquid fuel fires, and the extinguishment of fires inside electrical cabinets [55]. Other applications include the suppression of mine explosions [7, 8], and explosion prevention of pressure vessels containing liquefied petroleum gases [17].

While the application of water mist technology has proliferated, the physics of flame suppression, the flame suppression mechanism, and the most optimal water droplet size configuration, is poorly studied.

It is the aim of the present study to elucidate the physics of flame suppression including identification of the main mechanism of suppression, and the most optimal spray size configuration for flame suppression.

Many authors have touched on the elements for studying flame suppression. The only detailed study of flame speed variation with increasing water droplet concentration has been carried out by Mitani et.al. [38]. However, the main goal of their study was not to measure the effect of water mists on flame propagation.

2

The authors generated a water mist with a spray mass median diameter of 4.7 μm. By applying an increasing concentration of water spray to a rich ethylene and air flame they were able to measure the variation in flame speed. The flame speed as a fraction of the initial flame speed is shown in Figure 1.1.
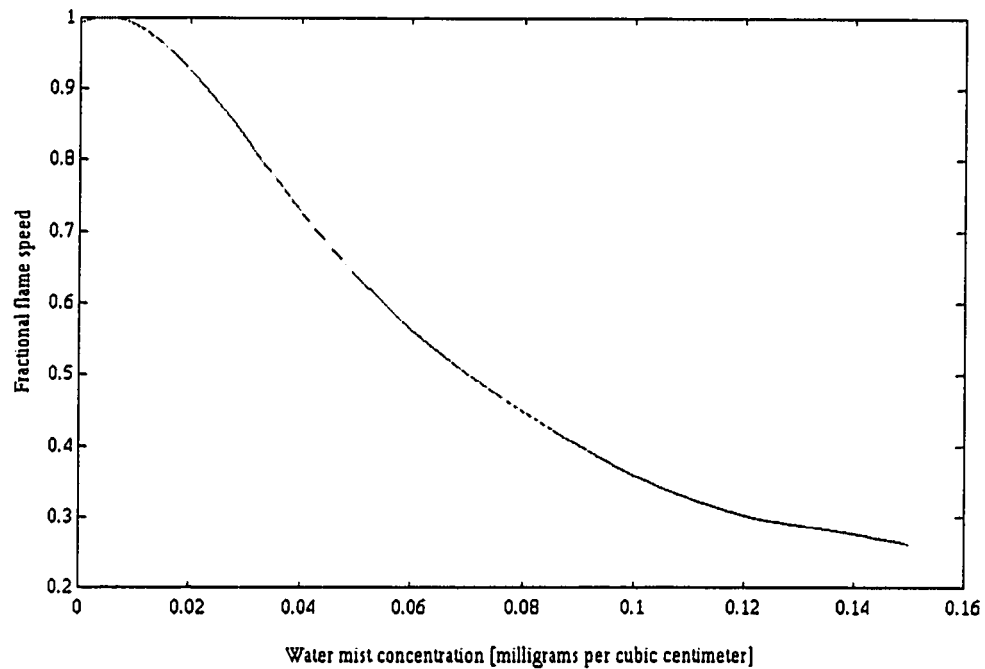
Figure 1.1: Flame speed variation for a rich ethylene flame.

The data from Figure 1.1 is of limited scope, and the present study expands the experimental parameters to varying concentration of water droplets and varying equivalence ratios covering both the lean and rich burning regions for a premixed laminar methane and air flame.

Sapko et.al. [6] also studied the effect of water sprays on flames. However, the authors did not conduct any flame speed measurements. The apparatus used by Sapko et.al. resulted in the flame propagating through regions of varying amounts of turbulence and varying concentrations of water spray. A consistent measurement of flame speed was therefore not possible.

The water sprays used in the current study were generated by a medical nebulizer. The spray mass median diameter was 3.75 μm, and the water droplet concentrations ranged from a mass fraction of 0.00088 to 0.012 in the reactants. The water droplet concentration was uniform as the spray entered the preheating zone of a conical flame. By keeping water droplet concentration constant in the preheat section of the flame, a detailed study could be conducted on flame speed variation with increasing droplet concentration. These experiments are described in detail in chapter three.

Sapko [6] calculated the optimal droplet mass median diameter to be 8 μm using a simple formula for droplet lifetimes. However, the droplet lifetime formula used by these authors is based on the premise that the droplets reach their boiling point inside the flame.

It will be shown in the current study that due to Stefan flow around the droplet, the heat and mass transfer is modified, and the droplets reach the wet-bulb temperature inside the flame. The wet bulb temperature is considerably lower than the boiling point for

water, and due to the dynamics of droplet motion, it is shown that droplet lifetimes can not be predicted using a simple formula.

An advanced computational model was also applied to the problem of flame and droplet interaction, to help elucidate the mechanisms of flame suppression. The model involved two-way coupling to account for interphase transfer of mass, heat, and momentum between the droplets and the gas phase. The numerical study is described in detail in chapter four.

To generate enough spray mass to extinguish the flames, a novel method of spray production was developed. By mixing water and supercritical carbon dioxide at high pressures, and expanding the mixture through a nozzle, fine water sprays with a high density of water mass were created. Due to time constraints on this work, this spray generation technique was not employed in the flame study. However, this method of droplet formation appears promising and parameters that affect its performance are explored in chapter five.

2. SURVEY OF RELEVANT LITERATURE

2.1 Flame quenching experiments

The effects of water on flames have been studied by many researchers. The first papers written on flames and water dealt with the flammability limits of methane and air mixtures with water vapour introduced as an inert [1, 2].

In 1955 a scientific study was conducted on the quenching of liquid pool fires by water mist [3]. The authors conducted tests on gasoline, kerosene and ethyl alcohol pool fires, with a water spray applied to the flames by an overhead nozzle. A set of experiments was also conducted on burning wood. The study resulted in tables of spray properties combined with information on whether the flames were extinguished or not. The overall conclusions were that flame quenching was due to the water diluting the air supply in the burning zone. The amount of dilution was in turn a function of the rate of water droplet evaporation. The authors considered the optimum droplet diameter for flame quenching to be 0.3 millimeters in diameter.

The research on liquid pool fires was expanded by Rasbash and Rogowski [4, 5]. In a set of experiments very similar to Braidech et.al. [3], Rasbash introduced the time lapse from the application of the spray until flame extinction as an additional parameter in the flame quenching analysis. The authors

conclusions were that cooling of the liquid surface to a temperature below the fire point resulted in extinction. A further conclusion was that smaller droplet sizes would extinguish the flames faster, and that the formation of steam in the burning zone, combined with the heat extracted from the flame for the evaporation process, played a role in quenching the flames. However, the air entrained into the burning zone by application of the spray was considered the major reason for extinction.

Sapko et.al. studied the process of quenching methane and air ignitions with water sprays [6]. The first part of the study only considered inerting a methane and air mixture by applying a water spray. A time delay was used to allow the mixture to stabilize after application of the spray. The mixture was sparked, and an observation was made as to the progression of a flame inside the testing chamber.

The authors also conducted quenching experiments. In these experiments a flame was established and allowed to propagate into an area of high water vapor concentration. The water spray was directed downwards inside the testing chamber, while the flame was allowed to propagate upwards towards the spray nozzle. They then observed whether the flame propagated beyond the spray cone of the nozzle, and this was used as the criteria for quenching. Unfortunately, no flame speed measurements were made. The authors concluded that to quench an established flame required a higher concentration of water spray than to prevent ignition of the

same combustible mixture. Increasing the droplet residence time in the reaction zone was considered an important aspect of reducing the flame speed. To calculate the optimum droplet size for flame quenching the authors used the formula,

$$R_0^2 = \frac{2t_0 K_a \ln\left(\frac{1 + C_p\left(T_a - T_b\right)}{\Delta H_v}\right)}{\rho C_p}$$

where R_0 is the initial droplet radius in centimeters, t_0 is the evaporation time in seconds, K_a is the thermal conductivity of the gas surrounding the droplet in calories per centimeter-second, T_a is the flame temperature in degrees Kelvin, T_b is the boiling point of the liquid droplet in Kelvin, H_v is the latent heat of evaporation in cal/gram, ρ is the droplet density in grams per cubic centimeter, and C_p is the heat capacity of the surrounding gas.

This equation was used to predict that a droplet with a diameter less than eight μm would be completely vaporized by a methane-air flame at $T_{flame} = T_a = 2185$ Kelvin. The authors calculated that for a nine percent methane and air flame with a one millimeter reaction zone and a flame speed of approximately 230 centimeters per second, the contact time between the droplet and the flame was approximately 0.43 milliseconds. This figure was used for the droplet residence time when calculating the maximum

8

allowable droplet diameter of eight μm. The recommendation was to keep the water droplets as small as possible to make the flame quenching system more effective.

Mitani and Niioka [38] conducted research into the rapid extinction of flames by adding alkali metal compounds imbedded in water droplets, to the gas stream. By generating a water mist with a mass median diameter of 4.7 μm, and passing the mist through a fuel rich ($\phi = 2$) ethylene and air flame they were able to measure the flame velocity, and the variation in flame velocity with increasing mist density. They found that they could not cause extinction by using water alone. When they added $NaHCO_3$ to the water droplets, they found that the flame would suddenly blow off once a critical value of the mist density was reached. The blowoff phenomenon was not observed using N_2, water, urea solutions, or the gaseous inhibitor CF_3Br as the inert. The alkali compounds apparently extinguished the flame if the particles resided in the flame long enough to decompose, and produce gaseous species to work as inhibitors.

Another area of research is the suppression of detonations by water sprays. Ng et.al. [7] conducted full scale studies in an experimental mine. A detonation wave was set up at one end of the test section. As the pressure wave hit troughs of water, small water droplets were dispersed. Upon arrival of the combustion wave the water mist would suppress the thermal wave, and thereby suppress the pressure wave. Similar research by Zhou and Lu [8] indicated

that weak explosions were not suppressed due to ineffective dispersal of the water barriers by the pressure wave.

Thomas et.al. [9, 10, 11, 12, 13] have conducted detailed studies on the physics involved in water mist suppression of combustion driven shock waves. The authors found that to quench a detonation, droplet evaporation alone is not adequate. A violent breakup of the water droplets by the shock wave is required to produce a micro mist. The shattering of water droplets into a mist enhances the ability of the water mist to act as a heat sink, and can lead to detonation quenching. The authors also found that in order to strip the droplets into tiny fragments, a violent explosion was required. In turn the mitigating effect on the explosion also became greater.

McCaffrey studied the effect of water sprays on jet diffusion flames [14]. By placing a pneumatic atomizing nozzle inside a pipe carrying the flammable gas, water sprays were introduced into a diffusion flame. To correlate the data from flame measurements with a characteristic of the spray, the mass median diameter was used. The mass flow rates of water and flammable gas were used as the experimental parameters to which flame temperature and heat release were correlated. McCaffrey found that the diffusion flames could be extinguished only at ratios of mass flow of water to flammable gas near values of four, five, and nine. No explanation of flame extinguishment was provided, and the author found that "... neither reduced heat release, extrapolated temperature nor the

rough guide to median drop size appears to differentiate these points...". This data is difficult to explain because the water and gas ratios where extinguishment occurs were all between values where the flames were not extinguished. However, McCaffrey [14] did speculate as to the mechanism of suppression as follows. Defining a reduced heat release rate, and assuming that the water spray is initially at 20 degrees Celsius, McCaffrey calculated a heat extraction rate by the water spray. By using a 1500 Kelvin flame for comparison, the author also concluded that the cooling capacity is doubled by using water droplets as the inert, instead of steam. The author also speculated that in addition to cooling the flame, smaller droplets would enter the reaction zone and affect the process of combustion. As a final hypotheses the author surmised that a diluent could interfere with the burning process by displacing some of the oxygen in the entrainment and mixing zone.

Watts researched the effects of water sprays on unconfined flammable gases [15]. It was shown that ethylene and air mixtures could be conditioned to a point where ignition could not occur, i.e. below the lower explosive limit, by applying water sprays. The main suppression mechanism was believed to be the entrainment of air into the flammable mixture by application of the water spray, thereby diluting the flammable gas. It was also found that a properly designed spraying apparatus could reduce the level of flammable gas to below the lower explosive limit in a matter of seconds.

Mawhinney et.al. [16] conducted a literature review and produced a table of the primary and secondary mechanisms of extinction. The primary mechanisms were heat extraction, oxygen displacement and radiant heat attenuation, and the secondary mechanisms were vapour and air dilution and kinetic effects.

Other authors have looked at the effect of water sprays on flames from an engineering perspective. For example, Schoen et.al. [17] investigated the engineering requirements needed to prevent a Liquefied-Petroleum-Gas vessel from bursting while being fully engulfed in flames from a propane fire. They found that by rearranging the spray nozzles they could not only prevent the tanks from exploding, but the overall flow rate requirement of water dropped by sixty percent.

Systematic data from quenching liquid pool fires and detonations is well established in the literature described previously. However, no systematic data exists for quenching laminar premixed flames with fine water mists. The only data similar to the current study is that of Mitani and Niioka [38]. However, the scope of their investigation was very limited. The current study expands the data to include variations in water droplet concentration at very low droplet loadings. The equivalence ratio is also varied over a wide range of flow conditions.

The theory of flame suppression using fine water mist is not well established. Previous work, described above, falls into two

12

main categories. The first category is suppression by heat extraction, and the second category is suppression by vapour dilution. The current study attempts to differentiate between these two modes of flame suppression. Based on the experimental and numerical data from the current study, a recommendation is also made from an engineering perspective, as to the design criteria for an efficient water mist flame suppression system.

2.2 Generating fine sprays

A brief review of methods for generating fine water mists with a droplet size range suitable for effective interaction with flames is provided here.

Chein and Lundgren [18] developed an aerosol generator capable of delivering aerosols ranging from one to ten μm in mass median diameter. The geometric standard deviation for the aerosol varied from 1.18 to 1.46, and the aerosol generation rate was 0.2 to 24 milligrams per minute.

Chen et.al. [19] developed an aerosol generator for generating very fine aerosols with narrow size distributions by using two virtual impactors in series. However, the apparatus was only tested for solid particles of oil shale, talc and fly ash.

Other authors describe various devices for generating aerosols such as the spinning disc aerosol generator [20], the

13

orifice aerosol generator [21], the ultrasonic nebulizer [22], the jet nebulizer [23], and the swirl injector nozzle [24].

Another technique for generating fine sprays is based on supercritical fluids. Sievers [25] has developed a technique for generating fine sprays by combining a solute (e.g. water) with a supercritical solvent, such as carbon dioxide. By mixing an aqueous solution with supercritical carbon dioxide in a mixing tee, and expanding the mixture through a small orifice, a very fine mist of the aqueous solution is created. Droplet sizes with a mass median diameter of three micrometers or less can be generated, depending on the properties and concentration of the solute. The apparatus and techniques are detailed in [26, 27, 28, 29].

A general review of the application of supercritical fluid technology can be found in [30, 31].

The physical properties of the water and carbon dioxide system has been explored in detail by [32,33]. The authors mainly concentrate on the solubility of carbon dioxide in water, and the solubility of water in carbon dioxide. Chun and Wilkinson [34] studied the effect of carbon dioxide on the interfacial tension of water, while Peck and Johnston [35] developed a theory for calculating the interfacial tension.

As the droplets are sprayed from a fine nozzle they deform and break up. While the theory of droplet production by supercritical fluid expansion is incomplete, the theory of droplet

break-up is well established and is reviewed in great detail by Faeth et.al. [36].

The current study expands on the work performed by Sievers et.al. [25]. A systematic investigation is conducted to elucidate the mechanism of spray creation for supercritical fluids. The experimental data is expanded over a wide range of parameters, and the effect on the water spray is recorded.

2.3 Modelling droplet and flame interaction

Mitani [39] developed a theory to determine the effect of inerts (particles and sprays) on flame speed. Mitani was able to develop an explicit expression for calculating the flame speed, based on two non-dimensional parameters. The first parameter is a measure of the fineness of the particles suspended in the flame, and the second parameter is a measure of the virtual heat capacity of the particles.

To consider the effect of inert gases Sermange [40] conducted a computational study of the extinction of hydrogen flames by increasing the amount of nitrogen in the mixture. The amount of nitrogen was increased until the flame velocity dropped to zero. The author found that at a velocity of seven millimeters per second, the flame temperature had decreased to 947 Kelvin for a stoichiometric hydrogen and air flame. This point, where the flame speed is almost zero, was considered the point of extinction.

Chen et.al. [41] conducted a numerical study using the universal flamelet code RUN-1DL. The flames were unstrained, premixed, freely propagating, stoichiometric methane and air flames, with water droplets added as the inerts. The authors found that the concentration of [OH] radicals decreased as the concentration of droplets increased, indicating that flame extinction is a possibility through the cooling effect of the water droplets on the flame.

However, the authors only considered a 30 μm droplet as their index case, with a reduced data set calculated for a 10 μm droplet.

Thomas [42] conducted detailed calculations on methane and air flames by varying droplet loading and sizes. By introducing water vapor into the reaction system, Thomas found that a dilution limit existed at 25 percent, beyond which a stable solution could not be obtained for the flame. The author remarked that this value agrees well with the established 26.5 percent extinction limit, from experiments. The author also tried to separate between the effect of decreasing flame speed as a result of heat loss versus a decrease in flame speed by vapour dilution. The author concluded that water droplets less than 20 μm in diameter behave as water vapour. An extinction point was determined for a 30 μm droplet at a droplet loading of 0.1 kilograms per cubic meter. The author speculated that the mechanism of extinction is the inhibition of exothermic reactions in the pre-heat zone.

The current numerical investigation is based on the flamelet code RUN-1DL [52]. A comparison is made between experiments, RUN-1DL, and a simplified droplet evaporation model. In contrast to the work described above, the current study is aimed at small droplets, and low droplet loadings. In addition, the numerical tools are used to attempt to differentiate between mechanisms of extinction.

3. EFFECTS OF WATER DROPLETS ON PREMIXED LAMINAR FLAMES

This chapter describes the methodology (3.1), the apparatus (3.2), and the diagnostic (3.3) equipment used to study the effects of dense fine water mists on premixed laminar methane and air flames. The results of the study can be found in section 3.4.

3.1 Experimental methodology

As described in the literature review, the inclusion of water droplets in the reactants of a premixed flame alters its propagation speed. There is essentially no data published on the effect of small droplets and very low droplet loadings, on laminar propagation speed of methane and air flames. To experimentally collect this information, an acceptable technique for measuring the flame speed had to be adopted. Of the techniques typically used, e.g. flat flame burners, stagnation flow burners, spherical flame growth rate vessels or conical flame angle techniques, it was decided that a conical flame burner provided the greatest flexibility.

By knowing the bulk flow velocity (U_L) and the cone angle (α) of the flame, the flame speed (S_L) can be calculated. This concept is shown in Figure 3.1.

18
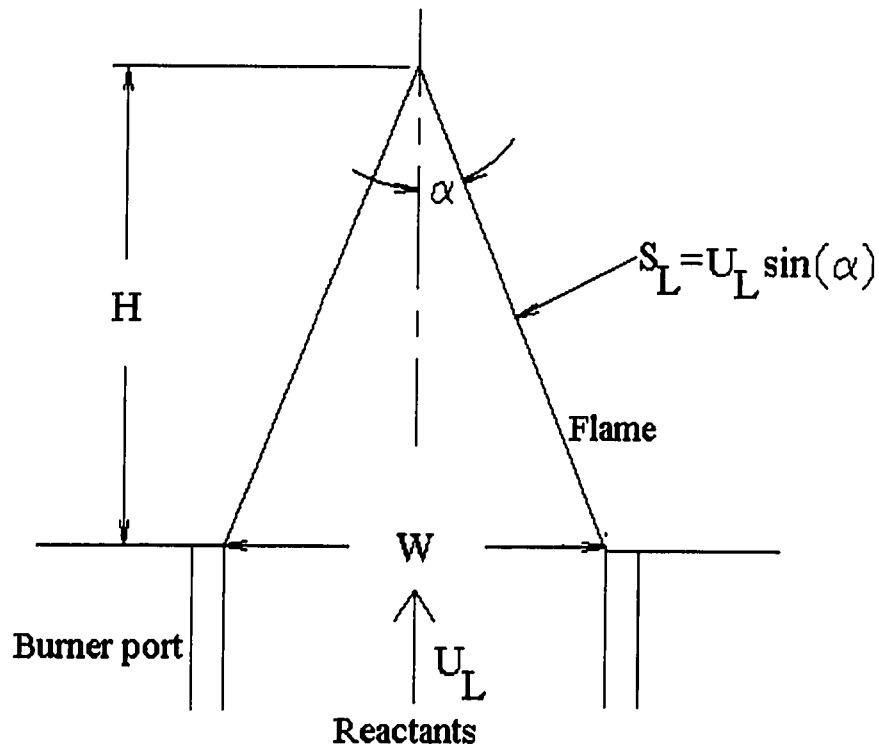
Figure 3.1: Calculating flame speed

Unfortunately, absolute flame speed cannot be determined using this method since the assumption of a one-dimensional flame is inaccurate. As well, there is also a question of where the flame truly resides. Depending on the measurement method, such as visible cone, schlieren visualization, or shadowgraph, different results for the laminar flame speed are obtained. The difference in measured flame speed can be as much as 10 to 50 percent.

However, obtaining absolute flame speed is not important here, since it is the trend in changing flame velocity that is important. The flame speed can always be scaled, e.g. by adjusting the flame speed data obtained at an equivalence ratio of one, and adjust it to match a reference value for a methane and air flame at the same equivalence ratio.

The above technique for measuring flame speed requires a gas stream of premixed fuel and air at a fixed flow rate, as described in section 3.2.1. Further, we need to measure flame angle, burner exit velocity, equivalence ratio, droplet size and number density, as described in section 3.3. To generate conditions suitable for the data measurements it was necessary to design a burner with uniform velocity profile at the exit, pilot stabilization to handle lean flames, and low turbulence intensity. The burner and experimental apparatus is described in sections 3.2.1 and 3.2.2 respectively.

3.2 Experimental apparatus

The experimental apparatus is described in two subsections. The first subsection consists of flow control, gas mixing, flow metering, and spray generation devices. The second subsection consists of the laminar flow burner.

3.2.1 Flow control, gas mixing and spray generation

A schematic of the setup is shown in Figure 3.2.
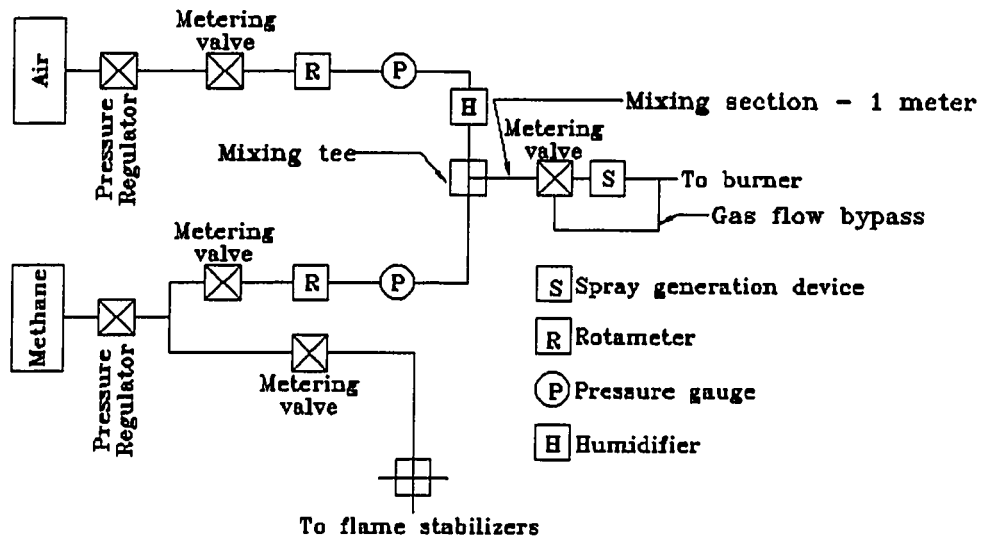
Figure 3.2: Flow control, mixing and spray generation apparatus

Compressed air from the building supplies the burner through a constant pressure regulator. The pressure regulator is set at 30 psig, which is the desired system pressure in the mixing section, and also provides good flow control through the metering valves.

Bottled, technical grade methane at 2500 psig is the fuel supply, and is also regulated to 30 psig with a two stage constant pressure regulator. The regulator output is split into two branches. The first branch is passed to a Nupro series "S" metering valve. The output of the valve is connected to a 3 way splitting tee which

21

in turn is connected to the flame stabilization ports on the burner. This approach allows for very fine adjustments of the amount of methane being fed to the flame stabilizer section, and facilitates attaching the flame to the burner for the whole range of flow rates and equivalence ratios. Details of the flame stabilizer are described in section 3.2.2.

The second branch of the fuel side is fed to a Nupro series "S" metering valve. The output from the metering valve is passed to a precision rotameter, and a pressure gauge. This equipment setup allows monitoring of the output pressure and flowrate from the rotameter. The metering valve allows very fine adjustments of the main flow of methane that goes to the fuel mixing section.

The air is fed through a rotameter and pressure gauge. A series "M" Nupro metering valve is used to control the main flow of air. The output of the rotameter is connected to a humidifier that raises the moisture of the incoming air to 100 percent relative humidity at a temperature of 40 degrees Celsius. The humidifier consists of a column of water heated to 65 degrees Celsius, which the air must bubble through. Humidification of the incoming air stream enhances droplet creation, and reduces droplet evaporation once the droplets have been added to the flow. The output of the humidifier is connected to the air and fuel mixing section.

The air and fuel mixing section is one meter of plastic tubing to allow mixing of the air and methane before reaching the spray generation device.

In order to vary the concentration of methane in air, i.e. control the burning velocity of the flame, the mixture ratio is set before the mixing section. This is accomplished by reading the pressure and flowrate from the rotameters. Details on the rotameter approach are described in Appendix A. The rotameter and pressure readings were used to get the appropriate mixture. A calibrated methane detector was used for the actual measurement of equivalence ratio. The methane detector is described in section 3.3.5.

The mixing section is attached to a flow control valve that sets the flow rate of the methane and air mixture going into the spray generation device. This is necessary to control the density of the spray of droplets being produced. The valve is designed to restrict the flow of gas into the spraying device while the remainder of the gas flow is bypassed and fed to the burner. This arrangement allows for a constant flow rate of gas entering the burner, and is necessary to stabilize the flame at the burner nozzle. When the bypass valve is fully closed, all the premixed fuel and air is fed to the burner, and is free of droplets. When the valve is fully open the maximum droplet loading is achieved.

To generate the spray, a medical nebulizer was used. A nebulizer was chosen based on the consistency and uniformity with which a spray was generated. It was also necessary to find a device that would have a long enough spray time to complete one set of measurements.

Three different models of nebulizers were considered, the Hudson Updraft II (Hudson RCI), the Upmist (Puritan), and the Devilbiss Pulmo-neb (Devilbiss). The nebulizers were attached to the burner, and spray measurements were done at the burner nozzle using the phase doppler anemometer described in section 3.3.1. The concentration measurement is described in more detail in section 3.3.2. The data collected from the three nebulizers is compared in Table 3.1.

Model	count mean diameter μm	mass mean diameter μm	mass median diameter μm	Concentration particles per cc
Hudson	2.90	3.22	3.75	230K
Upmist	2.63	2.81	2.98	127K
Devil	2.56	2.71	2.87	187K

Table 3.1: Nebulizer performance comparison

It can be seen from the table that the Upmist and the Devilbiss nebulizers produce almost identical mists, while the Hudson produces slightly larger droplets. The Hudson also produces a higher concentration of mist, which is desired for the flame extinguishing experiments. Based on the number density, the Hudson was chosen for the flame study.

Figure 3.3 shows the variation in spray concentration output from the Hudson nebulizer as the flowrate through the nebulizer is varied.
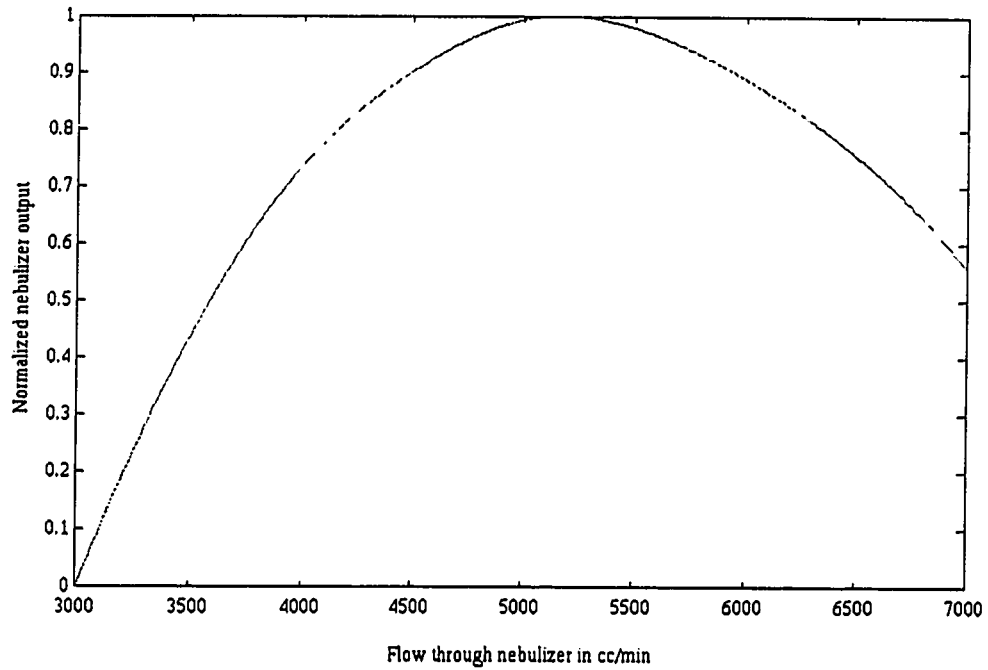
Figure 3.3: Spray concentration variation with the Hudson nebulizer

3.2.2 Laminar conical flame burner

Figure 3.4 shows a cross section of the burner without the turbulence inhibitor attached.
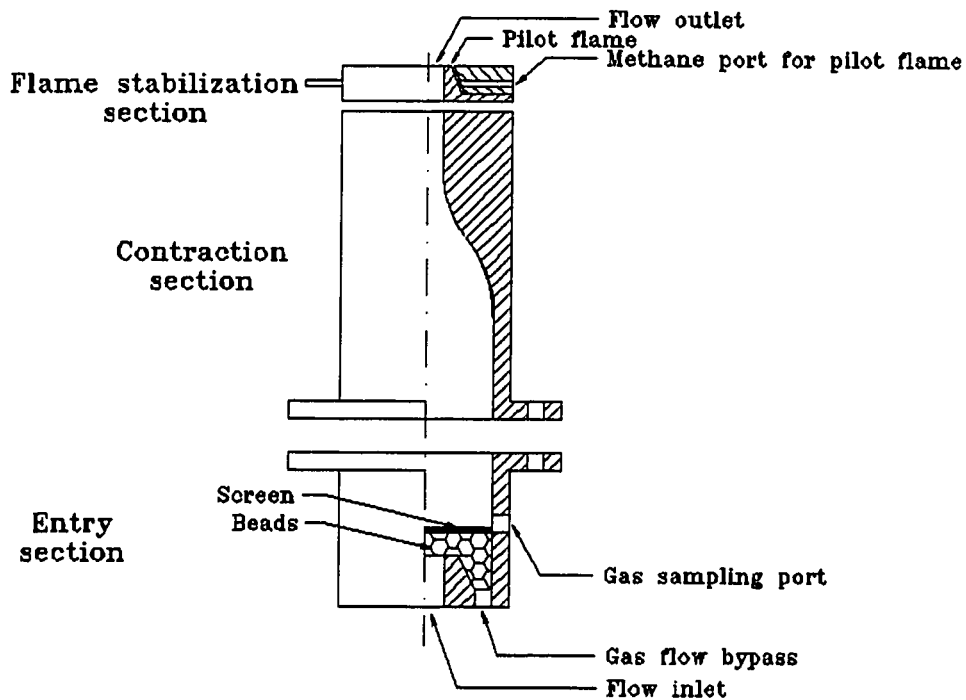
Figure 3.4: Burner without turbulence inhibitor

The burner is designed as a conical "bunsen" flame burner, where the flame is formed by a uniform stream of reactants issuing from the burner nozzle. To achieve these flow exit conditions the burner was constructed in three sections.

The lower entry section is filled with small glass beads to spread the incoming gas mixture across the burner diameter. Due to the beads obstructing the flow, some of the water droplets were lost in the entry section. This is the primary reason for measuring droplet concentration at the burner exit instead of at the exit of the spray generation device. It was also found that the flow of premixed gases and water droplets in the lower part of the burner created unacceptable levels of turbulence in the flow. The

turbulence was enough to make the flame unsteady, and the conditions unsuitable for measuring the laminar flame speed. The glass beads helped decrease the turbulence level, but a screen was needed to eliminate the vortex shedding from the glass beads. The mesh spacing was chosen so that the vortices induced by the mesh itself would disappear before reaching the contraction section. Adding beads to the bottom of the burner was also a safety measure to ensure that a possible blowback of hot gases would not propagate down the mixing section and cause an explosion. For higher flow rates of sprays it was found that it was not enough to add beads, but instead a turbulence inhibitor was designed, which is shown in Figure 3.5.
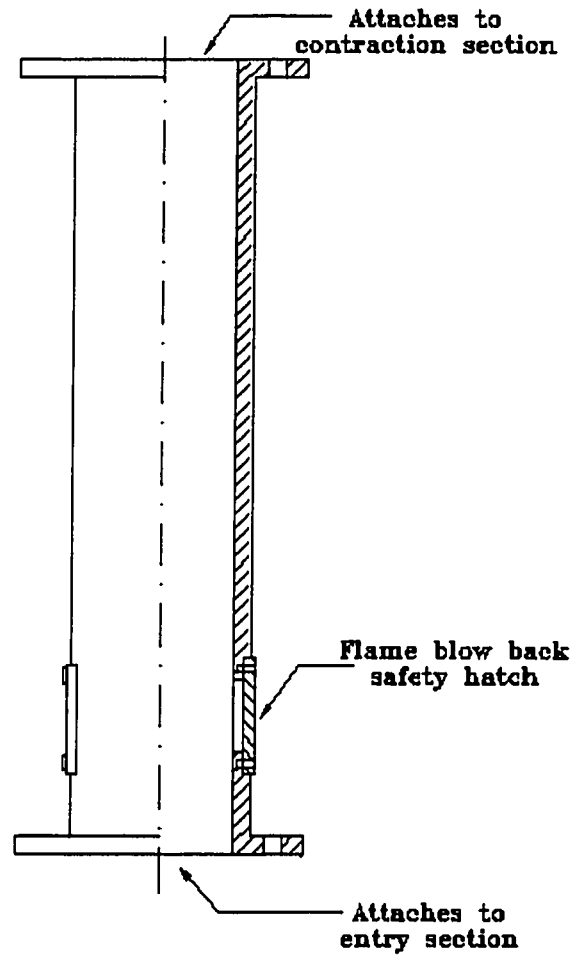
Figure 3.5: Turbulence inhibitor for burner

The turbulence inhibitor was designed to eliminate all turbulence induced by the spraying device, before the gas flow passes through the contraction section. The measured turbulence intensity from the denser sprays were around 30 percent in the lower part of the burner, and it was required to decrease the intensity to less than two percent to ensure a laminar flame at the burner nozzle. Hand calculations and a simulation in FLOW-3D resulted in the length of the turbulence inhibitor being twelve

inches. To verify the results of the calculations, a Plexiglas prototype of the turbulence inhibitor was built and tested with the burner. Measurements with the phase doppler indicated a 2.8 percent turbulence level at the nozzle with the full spray running. The Plexiglas also made it possible to study the flow of droplets and gas advancing through the burner. The turbulence level was found to be satisfactory for the flame as well, after testing the stainless steel turbulence inhibitor with the flame operating.

A safety mechanism was required to deal with blowback, since there is a considerable amount of flammable gas inside the burner with the inhibitor attached. This design is made up of two metal plates pressing on a seal recessed into the burner surface. Springs press on the outer surface of the metal plates, keeping them in place. Under normal operating conditions the two hatches remain closed by the spring pressure acting on them. When a flame propagates through the inhibitor, the pressure wave induced by the flame is enough to push the plates from the burner and vent the combustible gases.

The contraction section of the burner uniformly accelerates the flow to form a new top-hat velocity profile. For more detail on the design of the contraction section of the burner see Morel [43].

The velocity distribution over the exit of the burner nozzle was measured using the phase doppler anemometer while seeding the flow with water particles. It was found that the mean velocity

29

was constant across the entire burner nozzle, except for near the wall.

The flame stabilizer section consists of an annular space around the burner exit nozzle. Pure methane is fed into the annular space, and due to the induced annular flow of fuel, a pilot flame is established around the conical flame. The pilot flame helps stabilize the conical flame, particularly for low flame speeds as in the case of a lean flame.

3.3 Diagnostics

As described in section 3.1, the type of measurements needed are: gas flow velocity at the nozzle exit (3.3.1), spray concentration measurement (3.3.2), image of the flame to find the cone angle (3.3.3), and equivalence ratio (3.3.5). The experimental diagnostics is shown in Figure 3.6.
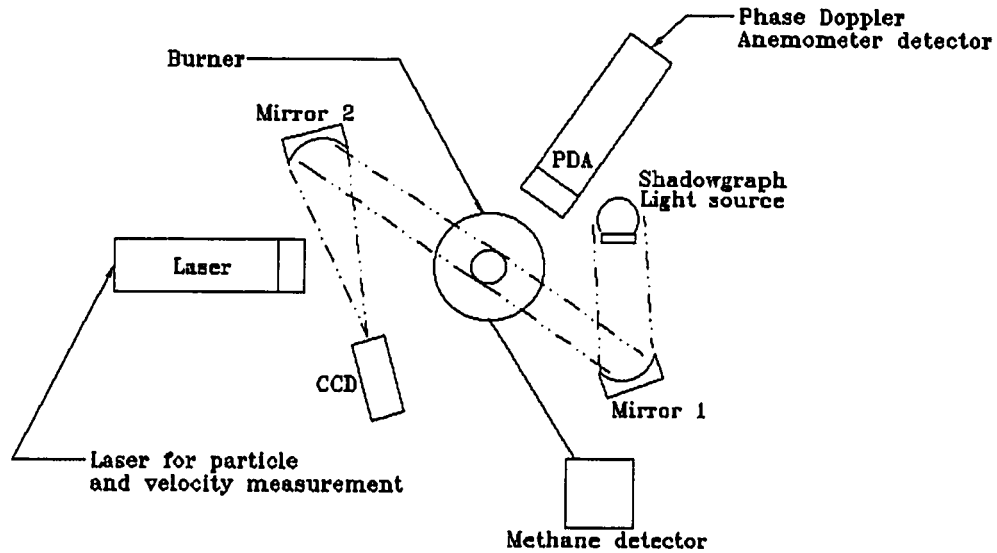
Figure 3.6: Experimental setup with diagnostic equipment

3.3.1 Velocity measurement

The velocity is measured with a phase doppler anemometer from Dantec Measurement Technology . The phase doppler anemometer is an extension of laser doppler velocimetry. The phase doppler incorporates additional photodetectors to analyse the size of a droplet, while the laser anemometer only measures the velocity of a particle. A phase doppler anemometer can therefore be more flexibly applied, and was also used in this study to determine spray characteristics.

The laser measurement point is positioned at the center of the burner nozzle, and five millimeters up from the nozzle exit. Passing a laser beam through a 2200 Kelvin flame surface leads to

beam steering problems. This can however be overcome by a high laser output and fine tuning the optics in situ as the experiment is running. It is also important to note that we only need to measure the velocity of the bulk flow, and that information on the spray quality can be collected without the flame present. Another issue to consider when measuring velocity with a laser anemometer is the sampling resolution. For the Dantec PDA system, the velocity is divided into 256 bins, and the resolution of each bin depends on the dynamic range selected. A test was devised with a constant property spray, in which the velocity sampling range was altered continuously to see what effect it would have on measured velocity, and as a secondary effect, on size measurement. The results are shown in Table 3.2.

Filter Bandwidth [MHz]	Velocity Range [m/s]	A/D resolution [m/s]	$U_{average}$ [m/s]	$U_{intensity}$ [m/s]	mass mean diameter [μm]
1.2	-0.8 to 2.4	0.0125	0.766	0.019	5.924
4	-2.7 to 8	0.0418	0.747	0.025	8.387
12	-8 to 24	0.125	0.695	0.056	11.015
36	-16 to 80	0.375	0.059	0.157	14.078

Table 3.2: A/D conversion characteristics of the Dantec PDA

It can be seen from the table that the effect on droplet sizing is much greater than on velocity. For the experiments, the two bandwidths used were 1.2 and 4. Between these two bandwidths there is a discrepancy in velocity of only 2.5 percent. The droplet size resolution however has a discrepancy of 41 percent. It is therefore acceptable to use the PDA for the velocity measurement, but droplet data can not be relied upon, unless all data is collected with the same bandwidth.

3.3.2 Spray concentration measurement

The phase doppler is capable of estimating the density of a spray. However, this estimate is extremely poor, when comparing data from an independent method with the phase doppler data. For the independent method the following procedure was developed.

A saline solution with a known concentration is prepared, and used in the nebulizer instead of water. The nebulizer is attached to the burner, and turned on for 5, 10 or 15 minutes. During this time, the spray at the burner nozzle is collected on a filter, and the flow rate of air through the spray generation device is kept constant. The filter is dried overnight, and weighed on a precision scale. Knowing the weight of the filter before and after spray application, the weight of the NaCl collected is determined. Using the concentration information, the amount of water spray that impacted on the filter in the given time frame can be

calculated. Dividing by the total spray time will yield the flowrate of spray in kilograms per second. Dividing the spray flowrate by the mass flow rate of air and water droplets yields the mass fraction of water droplets in the gas flow.

This method is more accurate than relying on phase doppler measurements, since we are dealing with easily determined physical quantities of mass and concentration. One systematic error that must be considered is that the collection filter cannot become saturated at the surface so that water droplets form and disappear into the burner, thereby losing spray mass from the total calculation. This condition was carefully monitored, and the collection times were chosen to reflect the density and flow rate of the spray at the burner nozzle.

3.3.3 Capturing flame images

Many methods were attempted to capture instant pictures of the flame. It was found that taking pictures in a dark room was sufficient for rich flames that had a high luminosity. However, for lean flames it was nearly impossible to see the flame at equivalence ratios of 0.7 and lower. Instead, a shadowgraph technique was used to enhance the image of the flame.

A shadowgraph is a scientific adaptation of the following naturally occurring phenomena: on a hot, sunny summer's day, looking at hot asphalt, or a metal roof, or a similar heat absorbing

34

material, it is possible to see "the heat rise" from the surface. This is a display of the density gradients in the air, with the sun acting as the light source required for illumination.

In the experimental setup shown in Figure 3.6, a highly luminescent light bulb from a slide projector, with focusing optics attached, was used as the light source. For the shadowgraph to work, the light beam illuminating the density gradients must be parallel. To accomplish this, the light from the slide projector is bounced off a concave mirror with a focusing distance of five meters. If the light source is situated at the focal point of the mirror, the reflected light from the mirror will be parallel. The focusing optics on the light source helped accomplish adjustment of the focal point, so that a parallel light beam could be obtained. To test for a parallel beam, a sheet of paper marked with the outline of the mirror was passed along the reflected beam. If the diameter of the reflected beam changed over the measurement distance, the focal point was readjusted.

The reflected light from the mirror, now made into a parallel light beam, is passed through the flame, and collected on a second mirror. The second mirror is used to refocus the light beam. At the focal point of the second mirror, a shadowgraph image of the burner is formed. This image should clearly outline the density gradients in the flame. However, the clarity of the image depends on the quality of the mirrors, and the power of the light source. The

greatest factor affecting sharpness in the image is the quality of the mirror adjustments to obtain a parallel light beam.

A conventional camera with high speed black and white film was placed at the focal point of the second mirror. It is very difficult to adjust the brightness of the shadowgraph to the film speed, and maintain adequate detail. It was also cumbersome to do a complete set of experiments, only to develop the film, and find that none of the pictures could be used because of under- or over-exposure, or lack of detail. To shorten the processing time of the flame pictures, and to improve the quality of the images, a digital camera with capturing abilities was used instead of the conventional camera. The digital camera was a Sony color CCD camera, attached to a video capture board. By being able to adjust the light conditions on the camera itself, and receive an image on a television monitor in real time, it was easy to set up the camera to adequately capture images with enough sharpness and detail.

3.3.4 Image collection and processing

The digital camera was attached to a computer with a video control board. In order to match velocity data with pictures in real time, it was necessary to design computer software to control the phase doppler and the image equipment. The phase doppler control program was made into the master controller. The image computer was configured as the slave, and was attached to the master

36

computer through a simplification of the RS-232 serial communication interface. At the same time a phase doppler velocity measurement was completed, a picture was taken. The two data streams were time and date stamped, and given a unique identification number so that phase doppler data and pictures of the flame could be linked in the data processing. Processing was done either off line as a batch sequence or on line in real time.

To obtain the correct geometrical data, a calibration picture was captured with a sheet of paper measuring three by three centimeters square, in place of the flame. This allowed a conversion factor to be obtained for the vertical and horizontal scales.

A computer program was designed to automatically eliminate background noise in the picture. It then performed a simple edge detection by proceeding vertically from the bottom plane and up, until the flame was reached. Once at the flame surface, the program would analyse the pixels in a small neighbourhood , and always move the "mouse" so that the flame surface was to the immediate left. In this way, the flame was traced out in a counter-clockwise manner. The tip of the flame was located, and the data set was split in two. A linear regression was performed on the data points, to find the slope of the flame surface on both sides of the vertical center axis.
The angle between the flame surface and the center axis was calculated on both sides, and an average was obtained.

3.3.5 Determining equivalence ratio

The equivalence ratio is defined as,

$$\phi = \frac{\left(Air \, / \, Fuel\right)_{\text{stoichiometric}}}{\left(Air \, / \, Fuel\right)_{\text{actual mixture}}}$$

As discussed in section 3.2.1, rotameters were used to set the equivalence ratio. However, while the accuracy of the rotameters was good, in order to verify the data, an independent measurement was needed.

A gas analyzer with real time detection abilities was purchased from Neotronics Inc. The Digiflam 2000 is a compact self-contained unit able to detect methane in two ranges. The lower range is from 0 to 100 percent of the lower explosive limit (LEL). The upper range is from 5.5 to 100 percent by volume. The instrument would automatically choose the appropriate range needed. The instrument was calibrated using a standard procedure described in Appendix B. The Digiflam was attached to the middle section of the burner by way of a three-way open tee. When no measurement was to be made, the third connection on the tee was left open to the atmosphere. The Digiflam takes a representative sample by using a small membrane pump. However, this suction was strong enough to make the flame flicker, and it was decided to measure the concentration of methane immediately before collecting any other data.

3.4 Results of the flame study

Figure 3.7 shows the flame propagation speed as a function of droplet mass fraction for two equivalence ratios. Figure 3.8 shows the propagation speed as a function of equivalence ratio for the extremes of loadings tested. The case of no droplets could not be measured since the phase doppler needs some particles to validate upon.
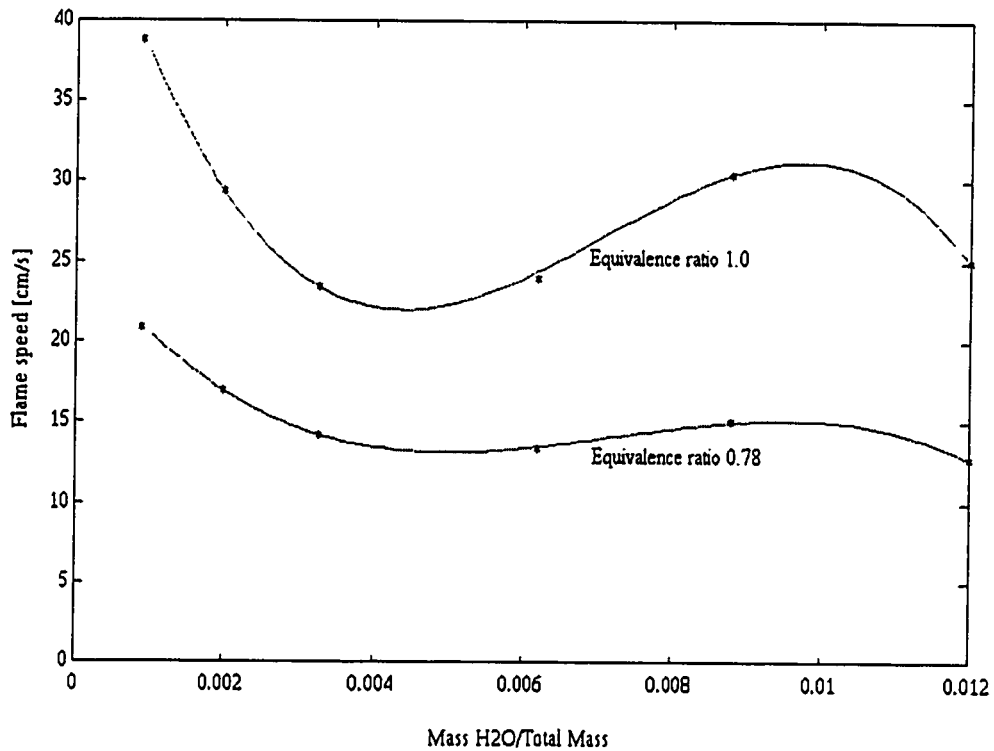
Figure 3.7: Flame speed as a function of droplet mass fraction
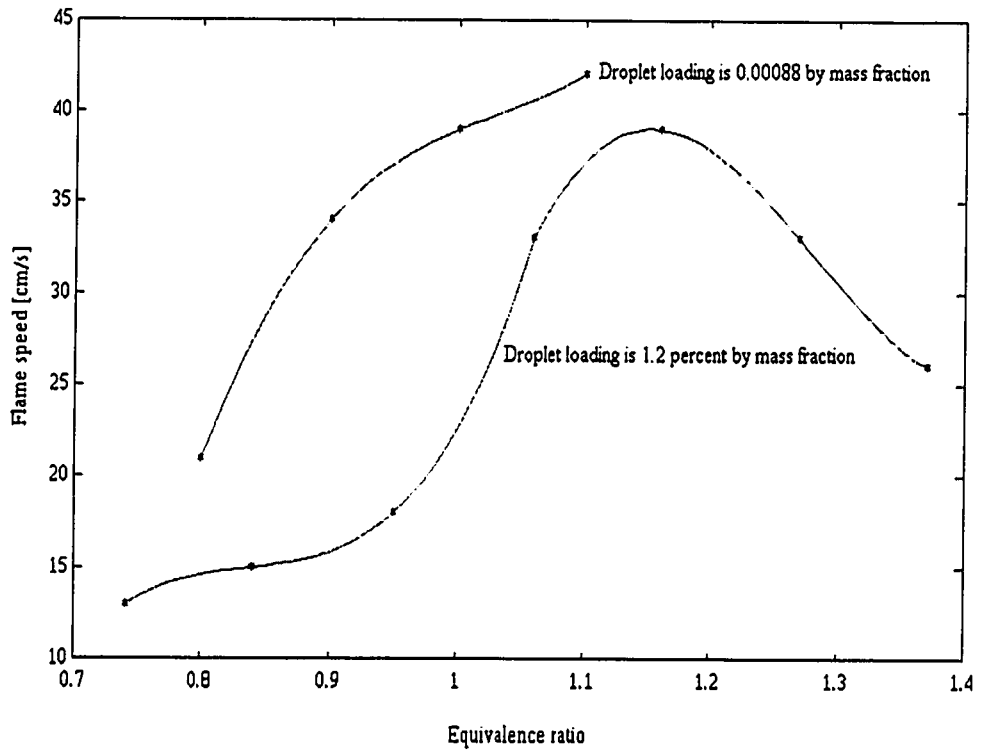
Figure 3.8: Flame speed as a function of equivalence ratio
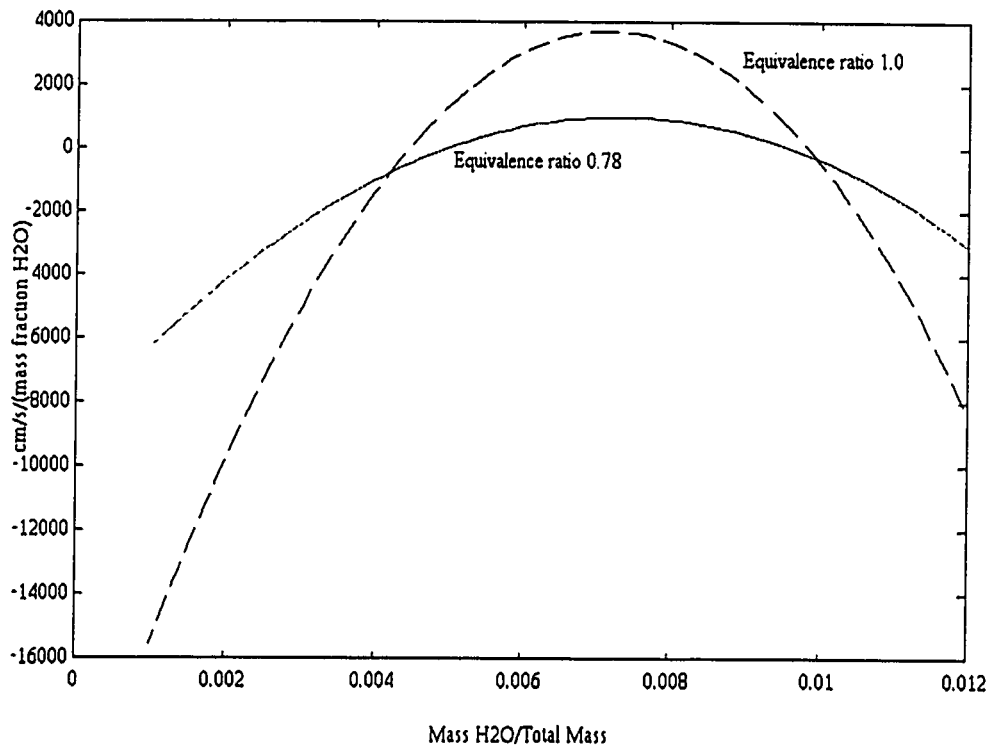
Figure 3.9: Rate of change in flame speed

As the droplet loading is increased the indication that the flame is being affected is very visual. This is particularly true for lean flames. The lean flames grow taller as the droplet loading increases. This is a direct indication that the flame speed is decreasing. To understand this effect we only need to look at Figure 3.1. If S_L is decreasing, with U_L remaining the same, the angle α has to decrease, which can only be accomplished by extending the height of the flame. A red glow was also observed with increasing droplet concentration. The red glow is radiation from water droplets or other particles in the flow. This glow would obscure the outer (visual) cone of the flame. However, since the

41

shadowgraph method is only concerned with density gradients, the red glow was only a concern when taking visual measurements of the flame.

For very small amounts of water droplets in the flow, the rich flames become buoyantly unstable, and can not be stabilized to allow for proper measurement of the flame speed. The data is therefore incomplete in this respect, and this is the reason for the "minimal droplet loading" curve ending just beyond the transition to the rich side of the flame.

The droplet data begins at a mass loading of 0.1 percent, which was found to be the lowest limit for which seeding of the flow would trigger the laser anemometer measurements.

It can be seen from Figure 3.7 that there is an initial decrease in flame speed. Figure 3.9 is used to find the point of zero change in flame speed. This occurs at 0.42 percent loading, for the stoichiometric flame, and 0.5 percent for the lean flame. It is surprising that the initial drop in flame speed is 42 percent for the stoichiometric flame, and 30 percent for the lean flame with equivalence ratio of 0.78.

Adding more water droplets to the flame actually increases the flame speed. Looking at Figure 3.9 again, the point for zero change in flame speed occurs for the second time at 0.92 percent droplet loading for the lean flame, and 0.98 percent for the stoichiometric flame . Both flames attain their points of zero slope in velocity, at almost the same droplet loading.

The increase in flame speed from the first minimum is 36 percent for the stoichiometric flame, and 17 percent for the lean flame. The overall decrease in flame speed from the no droplet flow is 34 percent for the stoichiometric flame, and 38 percent for the lean flame, at a droplet loading of 1.2 percent.

With local maxima and minima in flame speed coinciding for both flames, as evidenced by Figures 3.7 and 3.9, we can hypothesize that there are two processes working on reducing the flame speed. Up to the 0.45 percent droplet loading point, it seems that inert gas expansion from evaporation of the droplets is responsible for decreasing the flame speed. This is possible since the expansion from liquid to superheated water vapor involves a change in density of about 1000 times. Clearly, an expansion of inert gas that is rapid and massive would distort the chemical reactions by preventing fuel from reaching the reaction zone. By diluting the fuel and thereby changing the concentration gradients in space, the rate at which the chemical reactions progress would be reduced.

Starting at the 1 percent droplet loading, heat extracted from the flame by evaporating the droplets is the main cause for decreasing the flame speed. Heat being extracted from the flame lowers the flame temperature, thereby slowing down the chemical reactions, and resulting in a lower flame speed.

It is also interesting to note that extinction can not be brought on by inert gas (water droplet) expansion alone. Rather, it is the amount of heat extracted from the flame that will lead to extinction.

These hypotheses are supported in the literature. See for instance references [3, 4, 5, 6] who discuss both dilution and heat extraction as the main mechanisms for extinction. In the present study, there is an indication that the two theories are not mutually exclusive, as discussed by references [3, 4 ,5 ,6], but rather that they work at different times in the evolution of spray application to a flame. In chapter four, a more detailed discussion on the difference between the heat extraction and dilution mechanisms will be conducted, as we try to model the flame behaviour seen in this chapter.

4. NUMERICAL MODELLING OF DROPLET AND FLAME INTERACTION

This chapter describes the modelling of water droplets in flames. Sections 4.1 and 4.2 describe a simple model with one-way coupling of heat and mass transfer. Sections 4.3 and 4.4 describe a complicated model with two-way coupling and a more advanced treatment of the equations for mass, momentum and heat transfer. Section 4.5 summarizes the key features of this chapter, and compares the modelling results with experimental results from chapter three.

4.1 Description of the simple model

The quasi-steady conservation equations for mass, momentum, species and energy in the gas phase are as follows,

$$r^2 \rho v = r_d^2 \rho_w V_w = \frac{\dot{m}}{4\pi} = \text{constant} \qquad \text{[mass]} \qquad (1)$$

$$p \approx \text{constant} \qquad\qquad\qquad\qquad \text{[momentum]} \quad (2)$$

$$v\frac{\partial Y}{\partial r} = \frac{1}{\rho r^2}\frac{\partial}{\partial r}\left(\rho Dr^2 \frac{\partial Y}{\partial r}\right) \qquad \text{[species]} \qquad (3)$$

$$v\frac{\partial T}{\partial r} = \frac{1}{\rho C_p r^2}\frac{\partial}{\partial r}\left(\lambda r^2 \frac{\partial T}{\partial r}\right) \qquad \text{[energy]} \qquad (4)$$

and the boundary conditions are,

$$@ \; r = \infty \qquad T = T_\infty \qquad Y = 0 \qquad (5)$$

$$@ \; r = r_d \qquad \lambda \frac{\partial T}{\partial r}\bigg|_w = q_w = \rho_w v_w L = \frac{\dot{m}L}{4\pi r_d^2} \quad (6)$$

$$-D\rho \frac{\partial Y}{\partial r}\bigg|_w + Y_w \rho_w v_w = \rho_w v_w \qquad (7)$$

In equations (1) through (6) r is the radius from the droplet center, ρ is the density of the gas phase, v is the radial gas velocity, p is pressure, Y is mass concentration of water vapour, D is the diffusion coefficient of water vapour in the gas, T is temperature, C_p is the specific heat at constant pressure, λ is the heat conduction coefficient, and L is the latent heat of evaporation for the water droplet.

Equations (5) to (7) include the effect of Stefan flow around the droplet. The solution to the set of equations (1) to (7) can be determined analytically by multiplying the equations for species (3) and energy (4) by $4\pi r^2$, and using mass conservation to simplify the equations. Then,

46

$$\frac{d}{dr}(\dot{m}Y) = \frac{d}{dr}\left[\underbrace{4\,\pi r^2\rho\,D}_{k_1}\frac{dY}{dr}\right] \quad (8)$$

$$\frac{d}{dr}(\dot{m}T) = \frac{d}{dr}\left[\underbrace{4\pi\,r^2\frac{\lambda}{c_p}}_{k_2}\frac{dT}{dr}\right] \quad (9)$$

By introducing a transformation,

$$\alpha = \int_{r_d}^{\infty}\dot{m}/k_i\,dr \quad (10)$$

where k_i is either k_1 or k_2 as defined in equations (8) and (9). The equations for species and energy can be transformed to a readily solved equation:

$$\frac{d\beta}{d\alpha} = -\frac{d^2\beta}{d\alpha^2} \quad \text{with solution } \beta = C_1 + C_2 e^{-\alpha} \quad (11)$$

47

where β is either Y (species), or T (temperature). By making the assumption that the Lewis number, $L_e = \xi/D$ is a constant, where ξ is the heat diffusion coefficient defined as $\lambda/(\rho c_p)$, and D is the mass diffusion coefficient. The transformed equations with the boundary conditions $Y=Y_w$ @ $r=r_d$, and $T=T_w$ @ $r=r_d$ give us the mass transfer rate. The two expressions for the mass transfer rate are,

$$\dot{m} = 2\,\pi d\,\frac{\lambda}{c_p}\ln\left(1 + \frac{c_p}{q_w}\left(T_\infty - T_w\right)\right) \quad (12)$$

$$\dot{m} = 2\,\pi d\,\rho D\ln\left(1 + \frac{Y_w}{1 - Y_w}\right) \quad (13)$$

Furthermore, in this model the droplet behavior is assumed to be quasi-steady. This means that at each and every time step the droplet is in equilibrium with the gas phase with respect to pressure, temperature and species concentration. To find the mass transfer rate at every time step, the mass transfer rate equations above are required to equal each other, while solving for the droplet heat transfer rate q_w. In solving this equation, the vapour species mass concentration is related to the surface temperature of the droplet by $Y_w = fcn(T_w)$. The function used in the model is a cubic spline, and the saturation data was obtained from Cengel and Boles [47].

The droplet is assumed to be of uniform temperature, and any heat absorbed by the droplet is used to raise the bulk temperature. This is the lumped heat capacity concept, and its validity is for small droplets only. The limiting parameter is the Biot number, which is defined as, $B_i = hD/\lambda_{droplet}$, where the convective heat transfer coefficient, h, is obtained from the definition of Nusselt number, $N_u = hD/\lambda_{fluid}$. Assuming a constant Nusselt number of 2.0, the maximum Biot number obtained was 0.21, and the minimum value was 0.08. The limit for applying the lumped heat capacity method is a Biot number of 0.1. In the hot combustion products, it was therefore not appropriate to use a lumped heat capacity method for evaluating changes in droplet temperature, and this assumption was removed in the advanced model discussed in section 4.3. The following equations are the standard equations for droplet motion in a gas flow (see e.g. Crowe [51]).

By making the lumped heat capacity assumption, the equation that governs droplet temperature in time is,

$$m_d c_d \frac{dT_d}{dt} = \dot{m}(q_w - L) \quad (14)$$

The equations that govern the motion of the droplet are,

$$\frac{dV_p}{dt} = f\frac{18\mu}{\rho_p d_p^2}\left(U - V_p\right) \quad (15)$$

$$f = 1 + 0.15R_{ed}^{0.687} \quad (16)$$

$$\frac{dX_p}{dt} = V_p \quad (17)$$

The equation governing droplet mass,

$$\frac{dm_d}{dt} = -\dot{m} \quad (18)$$

The variables in equations 14 to 18 are defined as follows: m_d is the instantaneous droplet mass, c_d is the heat capacity of the droplet, T_d is the droplet temperature, q_w is the heat transfer rate at the surface of the droplet, and L is the latent heat of evaporation. V_p is the instantaneous velocity of the droplet, f is a friction factor, μ is the gas phase viscosity, d_p is the instantaneous droplet diameter, U is the gas phase velocity, and X_p is the distance the droplet has traveled from its starting point. The equations for m_d, T_d, V_p and X_p are integrated in time with an O.D.E. solver using the GEAR algorithm [56]. The integration time is the time to complete evaporation of the droplet, i.e., when the droplet mass m_d reaches zero.

The simple model was tested with gas phase data that was obtained from the flamelet code RUN-1DL [52]. The gas phase data pertains to a stoichiometric methane and air flame, from which the temperature and velocity field was extracted. Figure 4.1 shows the temperature in Kelvin, and the velocity in meters per second, as a function of flame coordinate in millimeters.
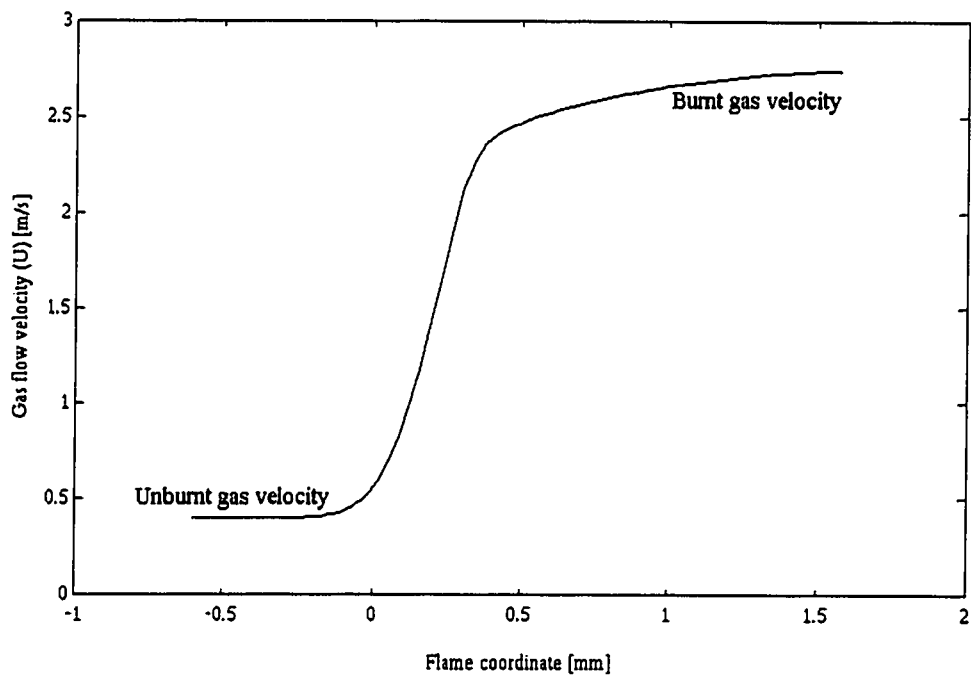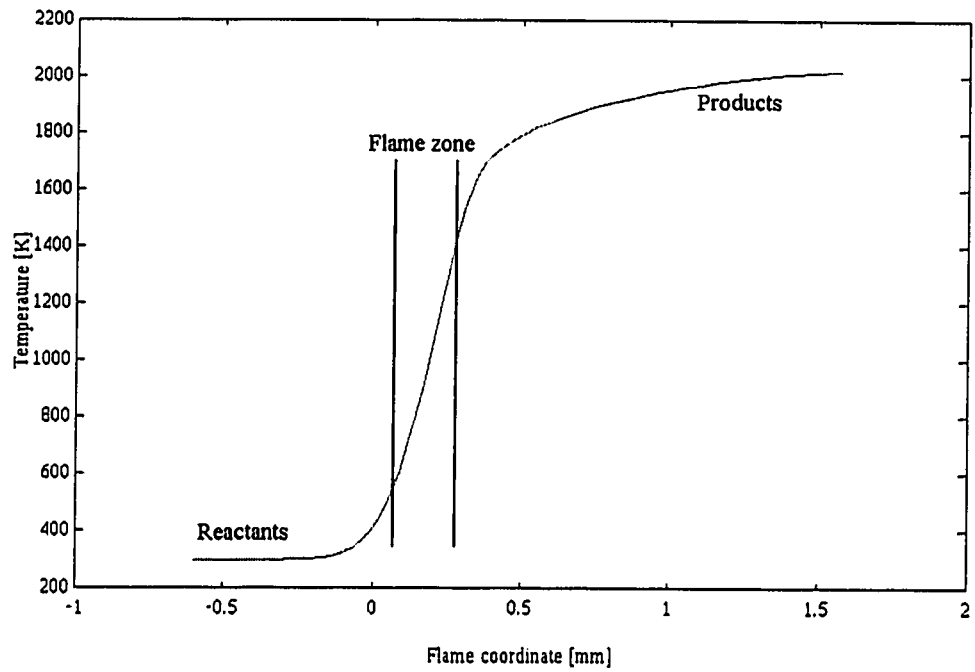
Figure 4.1: Gas phase temperature and velocity profiles

4.2 Computational results from the simple model

Figures 4.2, 4.3 and 4.4 show the progression of a single water droplet, of varying diameter, through the temperature and velocity field from a stoichiometric methane and air flame. Since we are only dealing with one droplet it was assumed that the gas phase profiles of temperature and velocity would not be affected. This is the assumption of one way coupling that was mentioned in the introduction to this chapter. The droplet is released in the preheat section of the flame, with an initial velocity equal to the gas flow bulk velocity, and an initial temperature equal to 298 Kelvin.
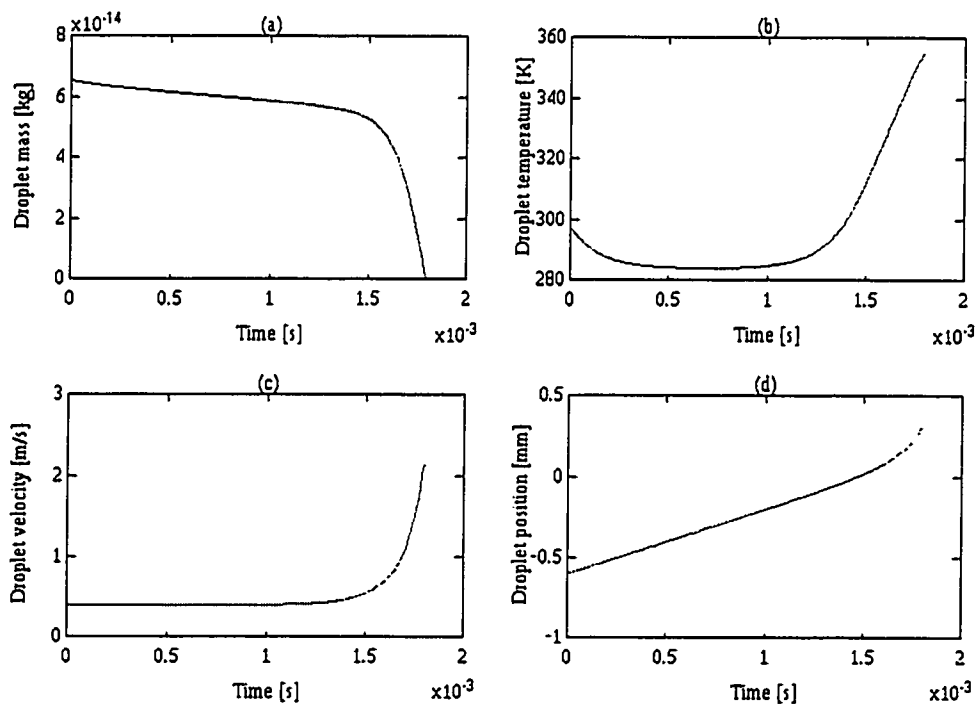
Figure 4.2: Five μm droplet progressing through the flame
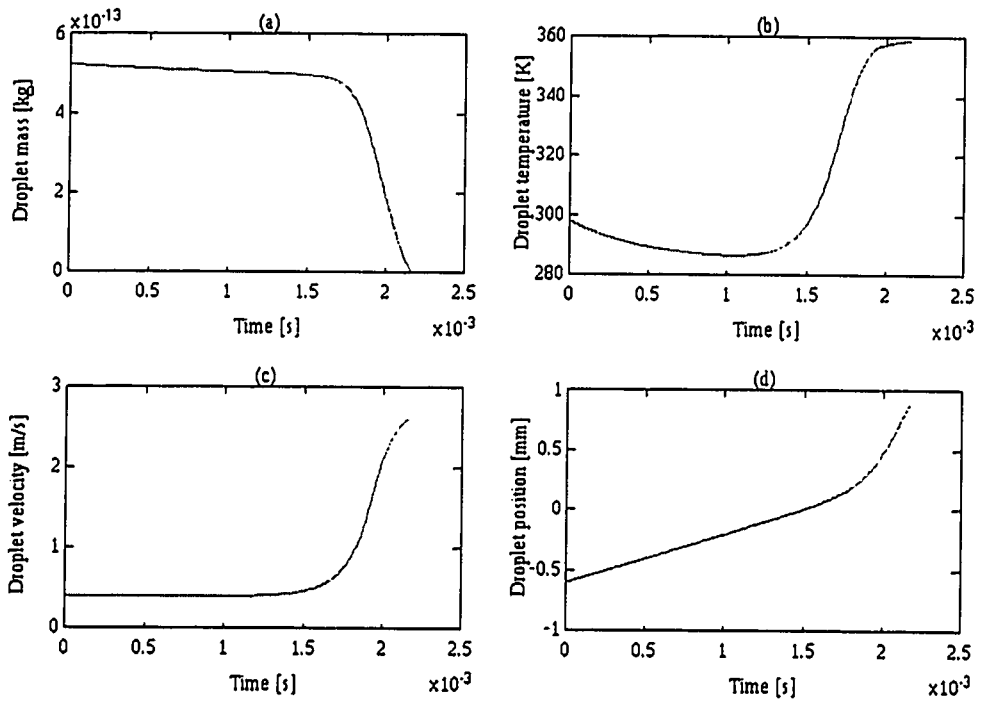
Figure 4.3: Ten µm droplet progressing through the flame
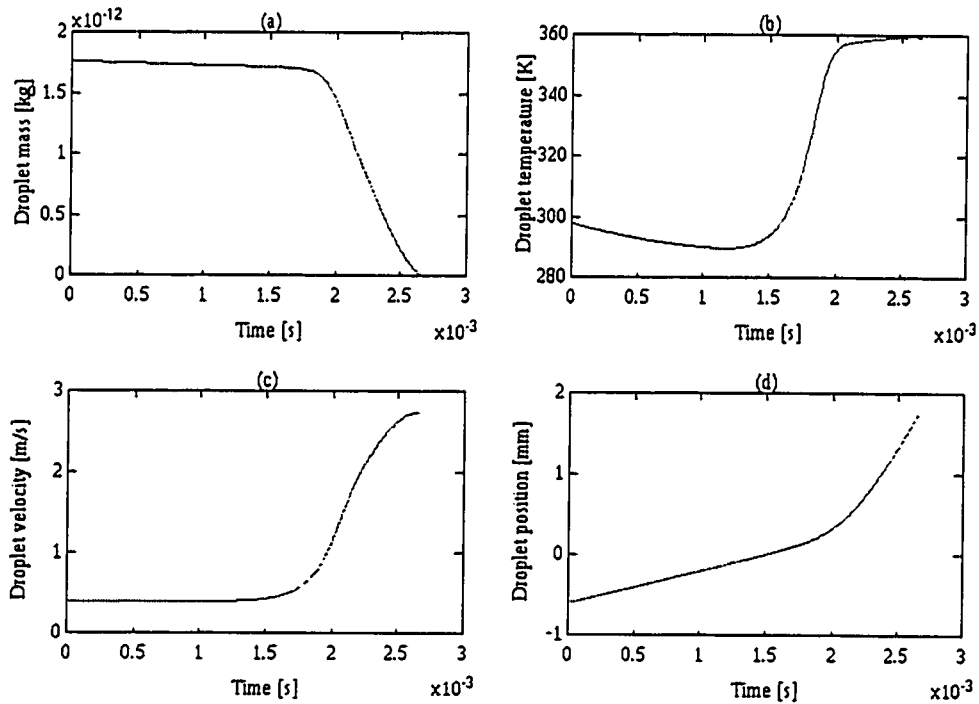
Figure 4.4: Fifteen µm droplet progressing through the flame

The results from the three computations can be combined in a graph of the evaporation times over the range of droplet sizes from five to fifteen μm. This is shown in Figure 4.5.
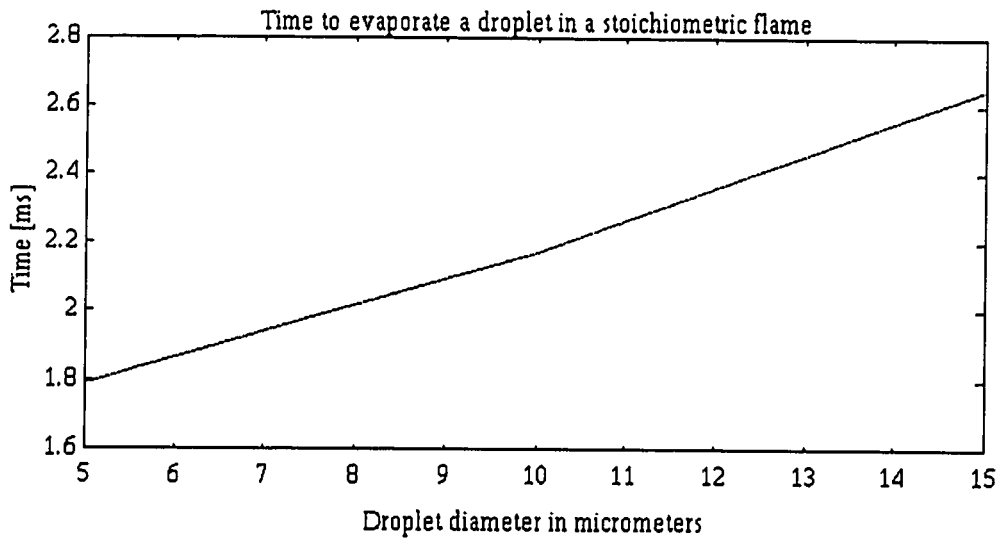
Figure 4.5: Droplet lifetime as a function of initial droplet diameter

To further understand the effect the droplets have on the flame, the location in the flame where the droplet life cycle ended is shown in Figure 4.6.
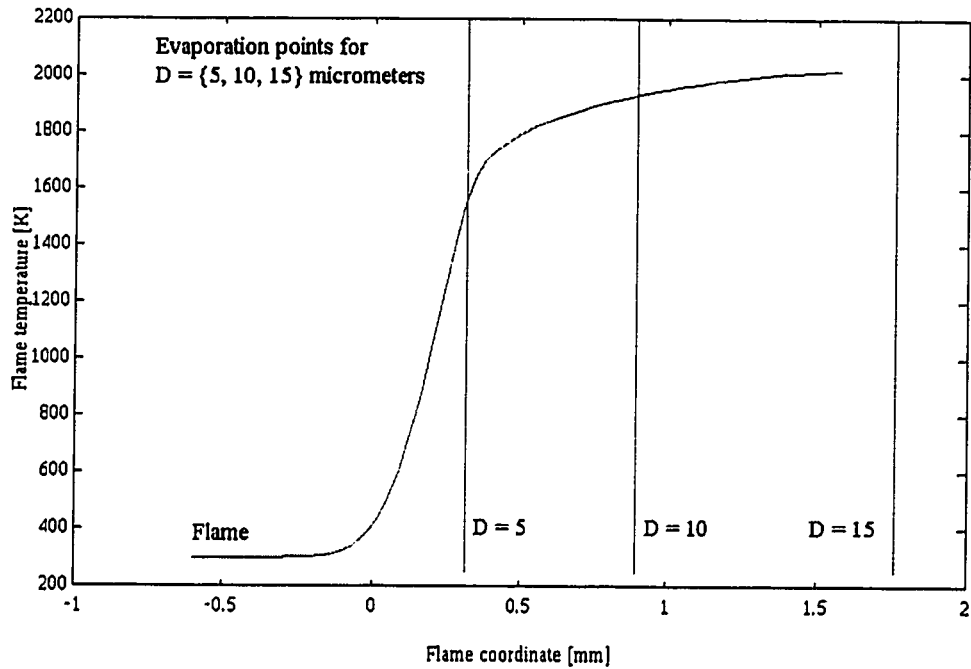
Figure 4.6: Location of droplet lifetimes in the flame

To explain the effect of the droplets on the flame we have to look at the structure of a laminar flame. A laminar flame can be grossly divided into three zones: preheat zone, reaction zone, and combustion products zone. This is shown in Figure 4.7, with the temperature profile from a stoichiometric methane and air flame added for reference.
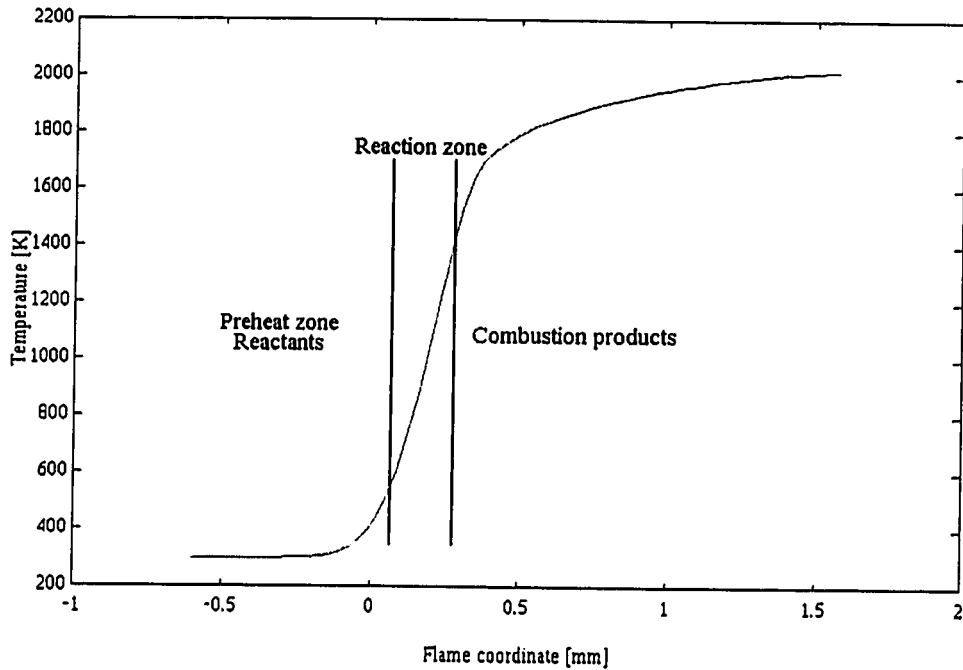
Figure 4.7: Flame regions

The reaction zone is characterised by a rapid increase in temperature where most of the chemical reactions occur. The preheat zone is a region where heat conduction from the hotter gases prepares the reactants for chemical reaction by raising their temperature. Following the reaction zone is a region where the gases gradually approach their equilibrium state.

It can be seen from Figure 4.6 that the 15 μm droplet evaporates far from the reaction zone, shedding most of its mass in the hot combustion products as evidenced by Figures 4.4 (a) and (d). At 2 milliseconds into the evaporation cycle, the droplet has lost about 3 percent of its mass, but has already passed through both the preheat and reaction zones of the flame. Hence, the

required effects of extracting sensible energy from the gas phase, or diluting the reactants prior to combustion, occurs too late in the structure of the flame to have any profound effect.

The 10 μm droplet also ends its life cycle in the combustion products. However, Figures 4.3 (a) and (d) indicate that the droplet upon entering the region of combustion products has shed over 60 percent of its mass in the preheat and reaction zones.

The 5 μm droplet ends its life cycle in the reaction zone, and sheds 100 percent of its mass in the preheat and reaction zones, with 50 percent in the preheat zone, and 50 percent in the reaction zone.

Referring to section 3.3, recall that our experimental results showed that low concentrations of water spray in the experiments had a drastic effect in lowering flame speed. In the experiments the droplet spray had a median diameter of 3.75 μm, and our model predicts that droplets in this size range should shed most of their mass in the preheat and reaction zones. It is likely that the reason we get such a drastic reduction in flame speed at low concentrations of water spray is due to the droplets mainly evaporating in the reaction zone. As a result, most of the droplet mass is converted into vapour in the reaction zone, leading to a diminished species concentration of methane and oxygen. Smaller gradients in reactant concentration in the reaction zone leads to lower reaction rates and a lower flame temperature, which in turn leads to a reduction in flame speed. However, when we increase

the concentration of droplets in the flow, the above argument does not explain our experimental results, since a higher concentration of droplets should lead to more water vapour in the reaction zone, and should eventually extinguish the flame. This was not the case in the experimental study.

The reason for this discrepancy lies in the computational model, which assumes we injected a single droplet into the flow. In the experiments we injected a spray of droplets, with varying diameters. As the droplets evaporate they interact and form a cloud of water vapour around them. This water vapour works to decrease the evaporation rate of the individual droplets, making them evaporate slower, and thereby not releasing most of their mass in the reaction zone. The cloud of water vapour is convected and diffused downstream, and the water vapour is superheated by the flame. Another problem is that as the gas temperature drops, the heat transfer to the droplets is reduced, and the smaller droplets do not evaporate in the leading part of the flame. Isolated droplets that would normally be expected to evaporate their mass early are now evaporating later in the flame, and the effect on the flame is thereby reduced. This would appear to be the reason why the flame does not easily extinguish as we increase the spray concentration. The determining factor instead becomes the ability of the water cloud to absorb heat from the flame, and to bring the flame temperature down to a level at which combustion can not be sustained.

4.3 Description of the advanced model

The purpose of the advanced model is to elucidate the effect of increasing water droplet concentration on flame speed. As discussed in the simple model, increasing water droplet concentration does not immediately bring on extinction. It is instead the ability of the water spray to absorb heat from the flame that will lead to extinction. It is not the total sensible energy extracted from the flow, or the final mixture composition (as predicted by equilibrium thermodynamics), but rather the local dynamics of the rates of evaporation inside the flame that determines if extinction will occur. The advanced model is a computer software package named RUN-1DL. It was created by Professor B. Rogg to perform computational studies on one-dimensional flames [37].

The program solves a set of ordinary differential equations, like equations 4.1 to 4.7, but with inclusion of source and sink terms that describe the effects of chemical reaction. Each chemical species in the flow has a balance equation to describe its advection, diffusion and rate of chemical reaction. The rates of chemical reaction are determined by modified Arrhenius rate equations for each of the elementary reactions in the mechanism.

RUN-1DL is able to handle many types of reaction chemistry. For this study a 4-step reduced mechanism for methane

combustion was used to calculate a freely propagating, one dimensional, laminar, premixed flame. The reaction scheme is,

$CH_4 + 2H + H_2O \rightarrow CO + 4H_2$
$CO + H_2O \rightarrow CO_2 + H_2$
$2H + M \rightarrow H_2 + M$
$O_2 + 3H_2 \rightarrow 2H + 2H_2O$

Table 4.1: 4-step reaction scheme for methane

To evaluate the 4-step scheme as opposed to the 25-step scheme, the results from a study on strained methane and air flames published by Rogg [44] are compared in Table 4.2.

Equivalence ratio	Strain rate at extinction for 25-step mechanism	Strain rate at extinction for 4-step mechanism	Difference in percent in strain rate at extinction
1	2275	2145	6.1
0.84	2830	2990	5.7
0.7	2975	3925	31.9

Table 4.2: Comparison of extinction criteria for 4- and 25-step mechanism of methane combustion

If we stay between equivalence ratios of 0.8 to 1.0 the error associated with choosing the 4-step mechanism remains bounded at less than ten percent. The 4-step scheme is easier to implement

numerically, and the computational time required is also less than for the 25-step mechanism.

For comparing numerical results from RUN-1DL with experimental results, the stoichiometric flame was chosen. A stoichiometric flame was chosen because the experiments showed a great variation in flame speed with increasing droplet loading, and greater variations in flame speed is easier to observe in the numerical results.

The droplet model is based on the modernised Sherwood and Nusselt number corrections. These corrections are required because the layer of water vapour surrounding the droplet modifies the spatial profiles for temperature and species concentration.

The Sherwood and Nusselt number corrections are defined as follows [52],

$$\widetilde{S}_h = 2 + [(1 + R_e S_c)^{1/3} \max(1, R_e)^{0.077} - 1] \frac{B_M (1 + B_M)^{-0.7}}{\ln(1 + B_M)}$$

$$\widetilde{N}_u = 2 + [(1 + R_e P_r)^{1/3} \max(1, R_e)^{0.077} - 1] \frac{B_T (1 + B_T)^{-0.7}}{\ln(1 + B_T)}$$

$$B_T = (1 + B_M)^{\phi} - 1 \qquad \phi = \frac{c_{p_F}}{c_{p_f}} \frac{\widetilde{S}_h}{\widetilde{N}_u} \frac{1}{L_e}$$

$$B_M = \frac{Y_{F_s} - Y_{F_\infty}}{1 - Y_{F_s}}$$

RUN-1DL fully incorporates two-way coupling. To properly calculate the effect on the flame by the droplets, and the effect on the droplets by the flame, an iterative procedure has to be used. RUN-1DL calculates the gas phase based on constant droplet profiles, and then reverses the order by calculating droplet profiles while holding the gas phase as a constant. This process is repeated until a converged solution is obtained.

4.4 Computational results from the advanced model

Figure 4.8 shows the concentration and temperature profiles for a stoichiometric methane and air flame, with a droplet loading of zero. The calculated flame speed is 39.8 centimeters per second.
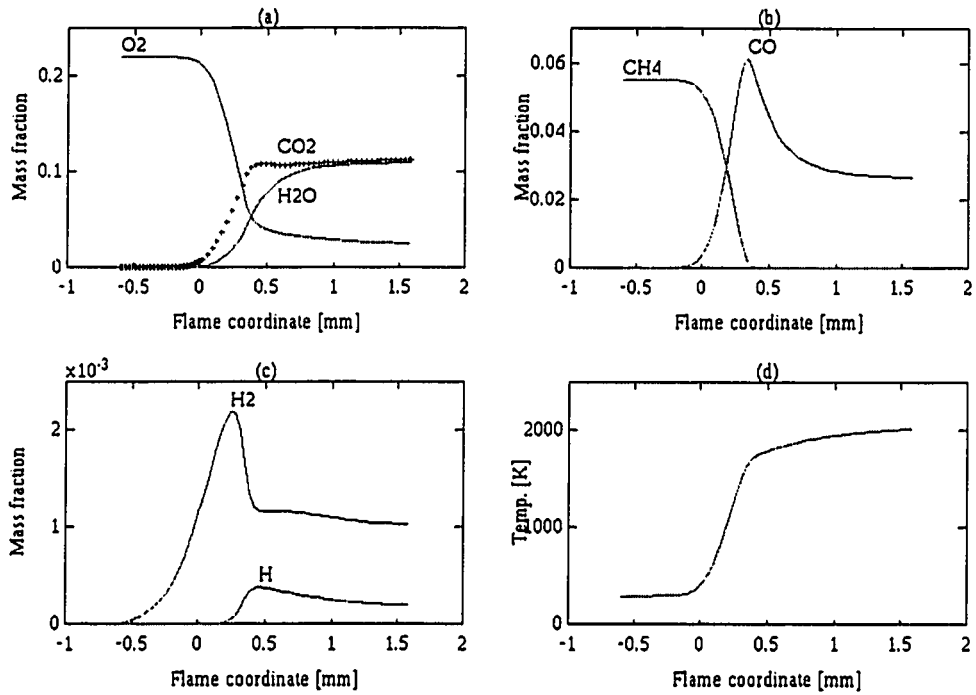
Figure 4.8: Profiles of flame properties

To compare the simple and the advanced model we can look at the process of evaporation for a 10 μm droplet. The simple model droplet evaporation is shown in Figure 4.9, and the advanced model prediction of droplet behaviour is shown in Figure 4.10.
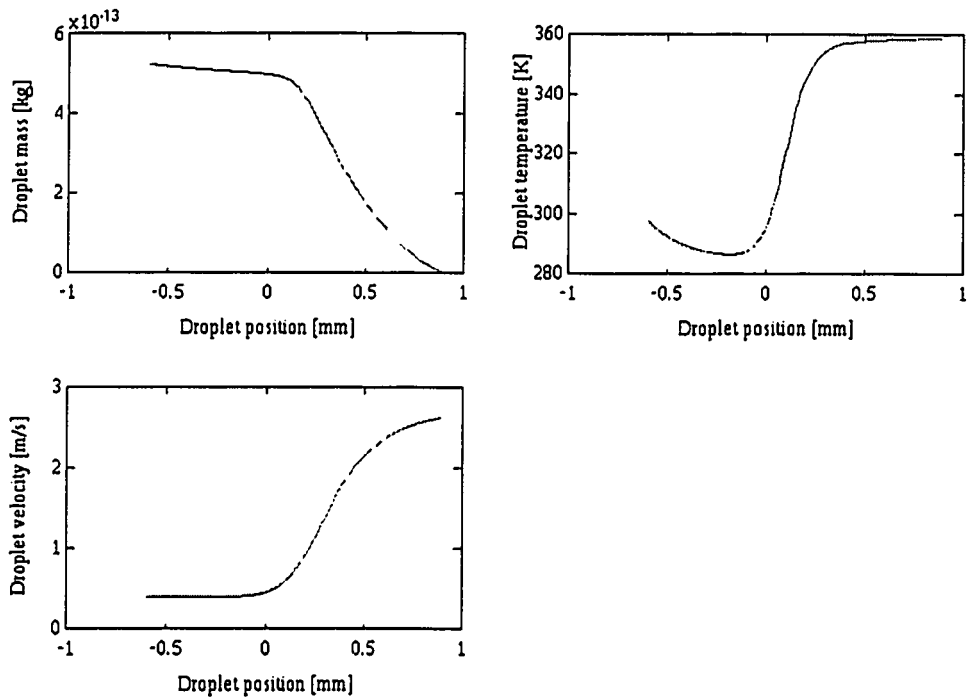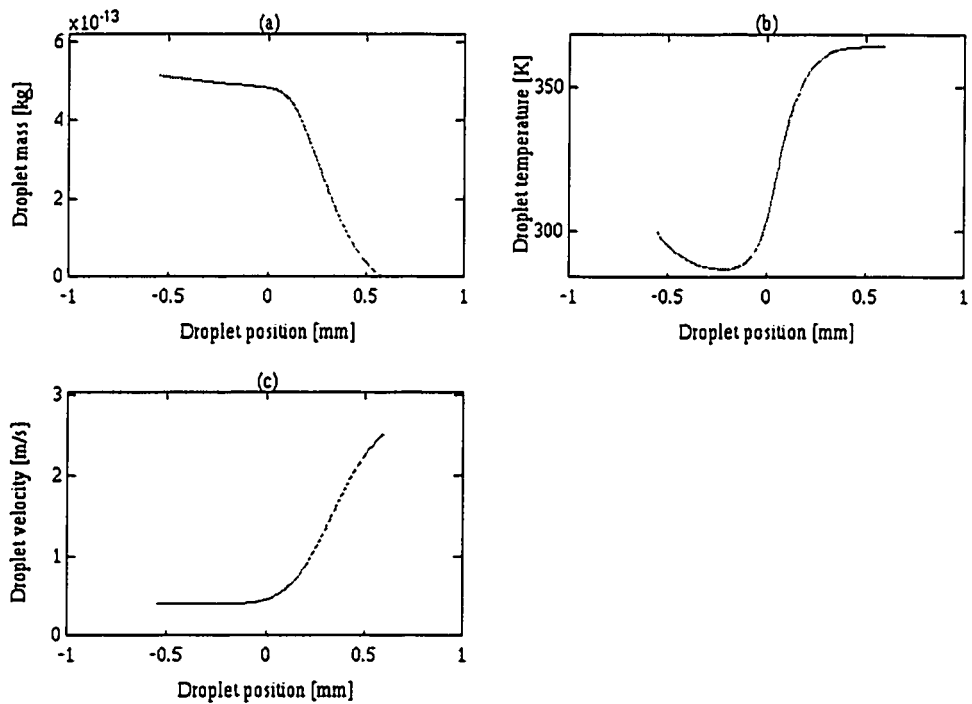
Figure 4.9: Simple model droplet evaporation

Figure 4.10: Advanced model droplet evaporation

In both cases, the droplet number concentration was near zero. Only one droplet was allowed to pass through the flame, and both droplets started out at the same initial temperature, velocity and position in the flame. The profiles for mass, temperature and velocity are very similar. Some droplet evaporation characteristics are shown in Table 4.3.

Characteristic	Simple model	Advanced model
Terminal position in flame	0.89	0.6
Maximum temperature attained	359	364
Minimum temperature attained	286	286
Maximum velocity attained	2.62	2.52

Table 4.3: Selected droplet evaporation characteristics

There is a clear agreement on every characteristic in the evaporation process, except for the evaporation rate. This results in a longer lifetime predicted with the simple model. The disagreement in predicted life time is 33 percent.

Figures 4.11, 4.12, 4.13 and 4.14 show the effect of increasing water droplet concentration from a monodisperse spray with a droplet diameter equal to 10 μm.
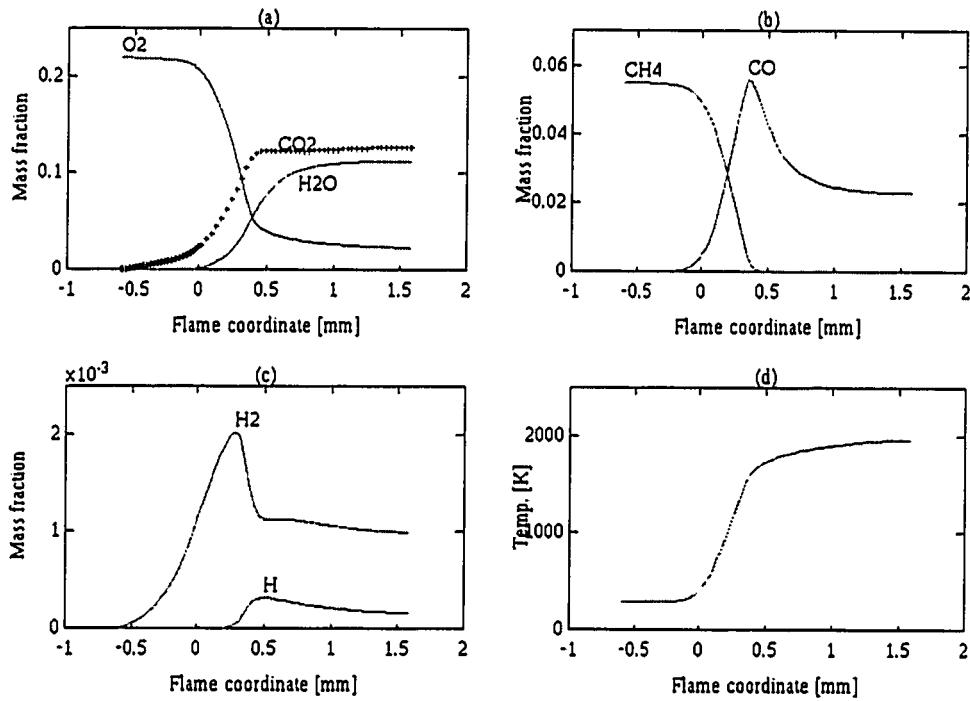
Figure 4.11: Profiles of flame properties for a droplet concentration of 1.5×10^{13} [No./m^3]
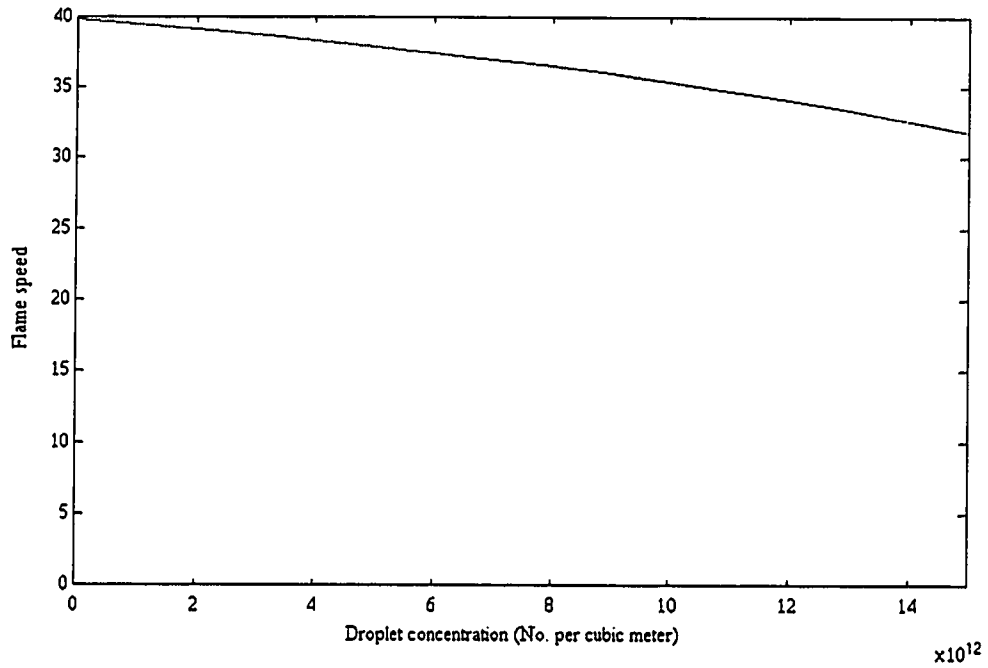
Figure 4.12: Increasing droplet concentration versus flame speed
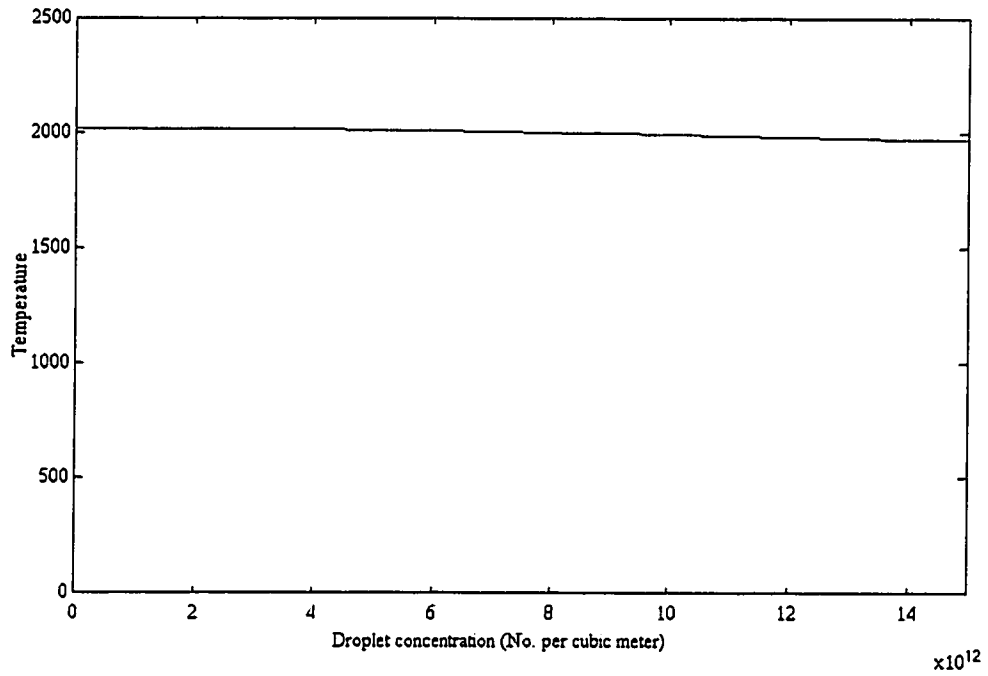
Figure 4.13: Increasing droplet concentration versus flame
temperature
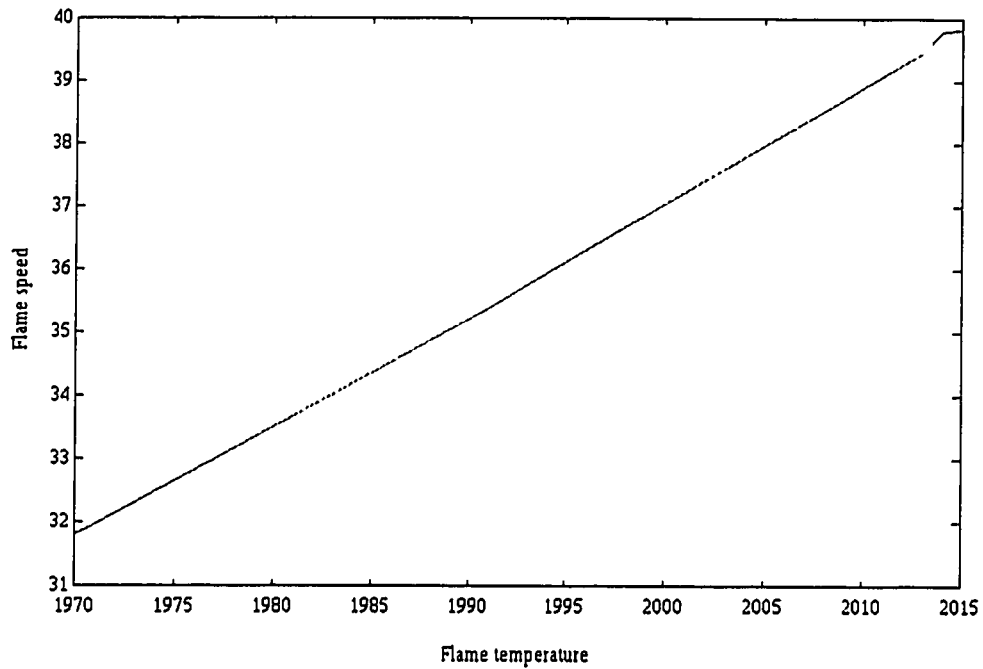
Figure 4.14: Flame temperature versus flame speed

No data could be obtained above a number concentration of droplets of 1.5×10^{13} due to stability problems with the flame code.

As a final comparison, a set of data was computed based on the experimental measurements. The droplet diameter in the experiments was $D_{median} = 3.75$ μm, and droplets this size were used for the following monodisperse droplet case run with the advanced model.

69
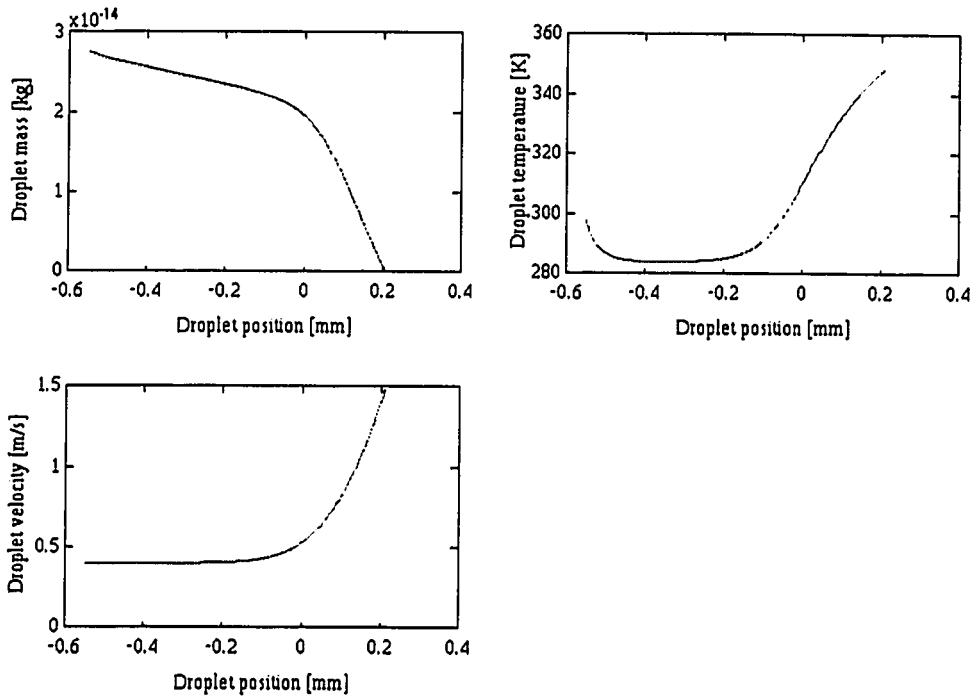
Figure 4.15: Simple model droplet evaporation for 3.75 μm droplet
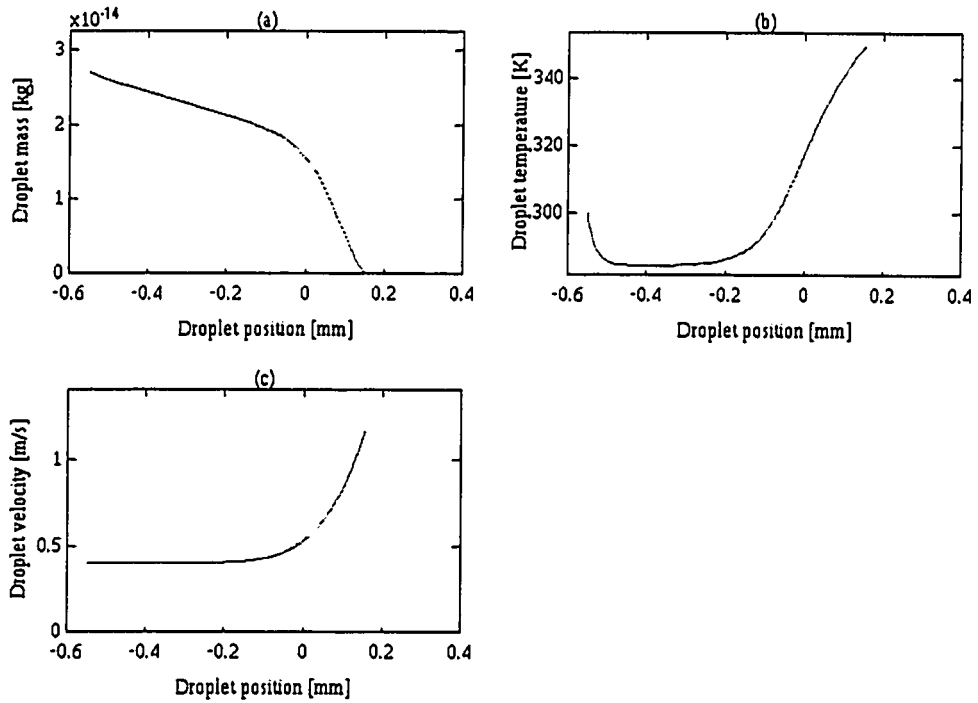
Figure 4.16: Advanced model droplet evaporation for 3.75 μm droplet

70

We can see from Figures 4.15 and 4.16 that the evaporation characteristics differ less for the smaller droplet than for the 10 μm droplet in Table 4.3. The advanced model predicts complete droplet evaporation at a flame position of $y = 0.16$, and the simple model predicts evaporation at $y = 0.21$. The difference is 24 percent compared with 33 percent for the 10 μm droplet. Referring to Figure 4.7, we can see that the 3.75 μm droplet evaporates in the first quarter of the reaction zone. Based on the data from the simple model, the droplet only sheds one third of its mass in the reaction zone, while two thirds is shed in the preheat zone. The advanced model predicts that only 1/6 of the mass is actually shed in the reaction zone, with the remainder in the preheat zone.

Figures 4.17, 4.18 and 4.19 show the flame profiles and flame velocity and temperature variation with increasing droplet concentration for the 3.75 μm droplet.
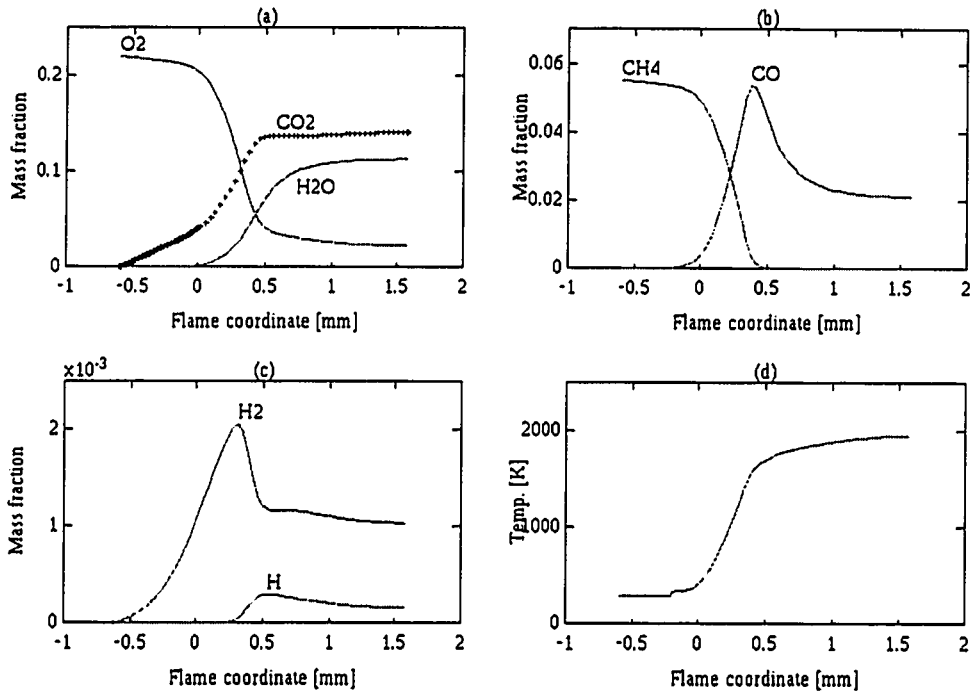
Figure 4.17: Flame profiles for a 3.75 μm droplet at a droplet concentration of $6x10^{14}$ [No./m³]
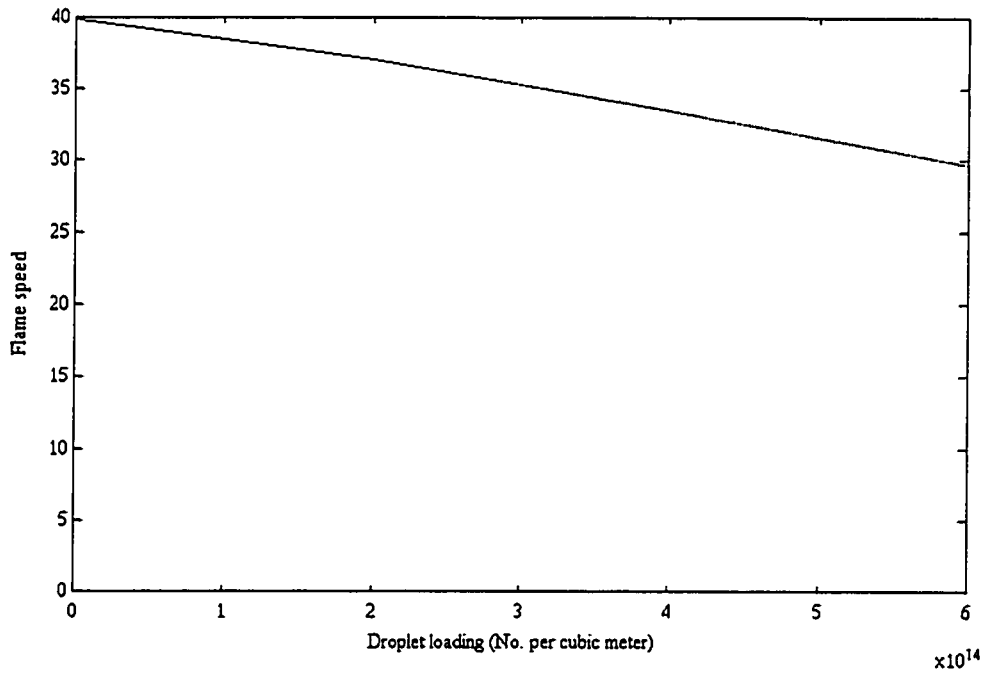
Figure 4.18: Flame speed variation with increasing droplet loading
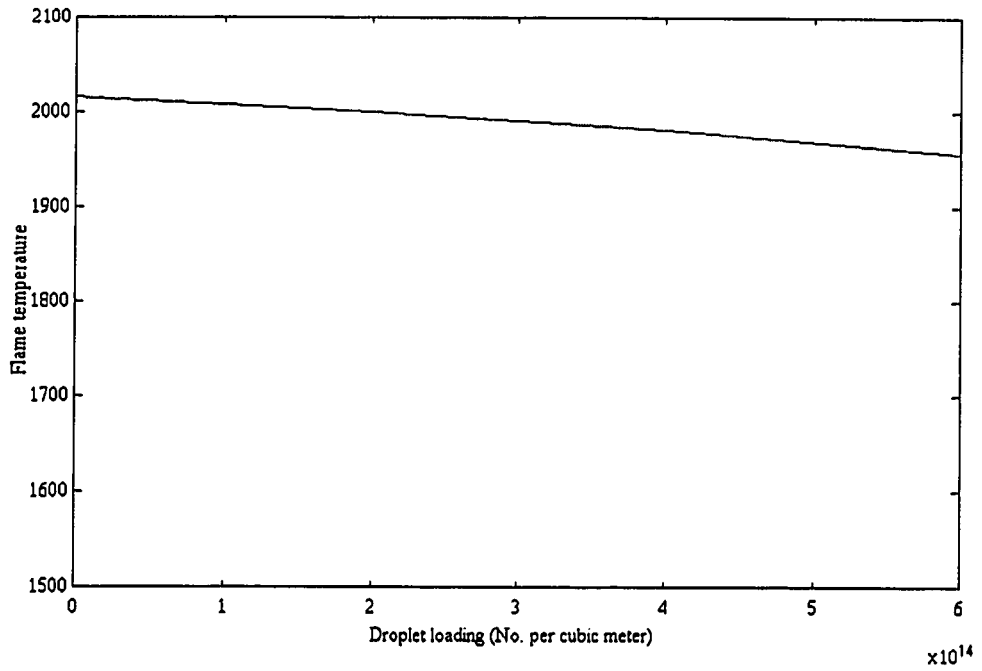
Figure 4.19: Flame temperature variation with increasing droplet loading
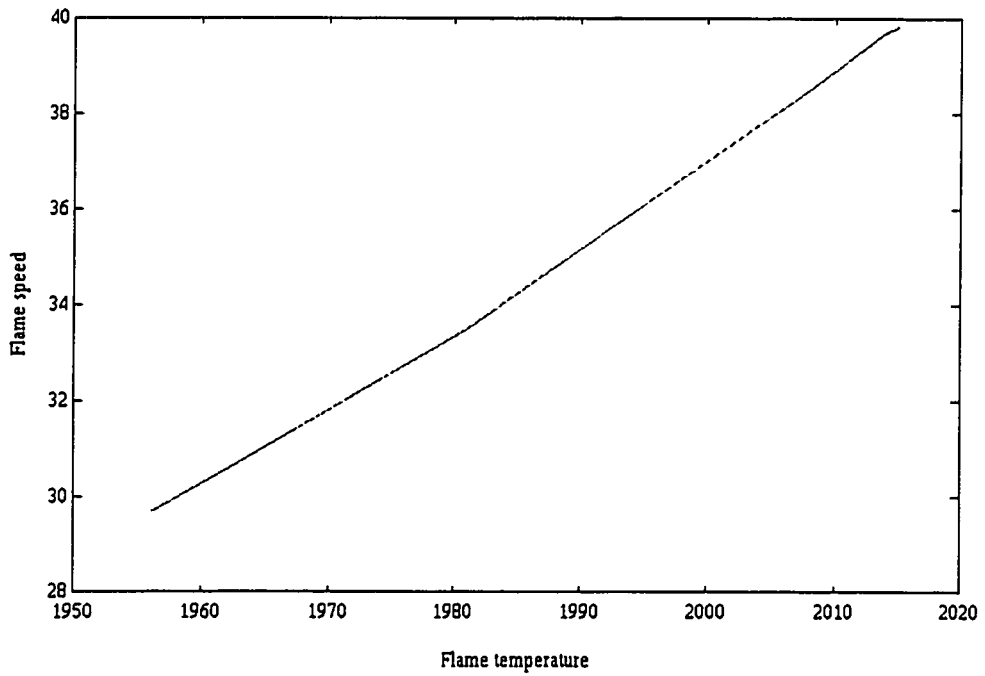
Figure 4.20: Flame speed variation with flame temperature

73

The flamelet code became unstable for droplet concentrations exceeding 6×10^{14} [No./cm^3], and a converged solution could not be obtained.

Table 4.4 summarizes two of the key comparisons between the 10 μm droplet case, and the 3.75 μm droplet case, as predicted by the advanced model.

Parameter for comparison	10 μm droplet	3.75 μm droplet
Concentration [No./m^3] required to yield a reduction in flame speed by 8 cm/s	1.5×10^{13}	4.5×10^{14}
Flame temperature predicted at a velocity deficit of 8 cm/s	1970	1970

Table 4.4: Summary of key features comparing two droplet simulations with the advanced model

Table 4.4 clearly indicates that the advanced model works on the total heat absorbed by the droplets from the flame. This is evidenced by identical flame temperatures for a velocity deficit of eight centimeters per second, but at a substantially higher mass concentration of water droplets for the smaller droplet case.

4.5 Conclusions on flame suppression mechanisms

Referring to Figures 4.10, 4.16 and 4.7 it can be seen that the smaller droplets evaporate in the reaction zone, while the bigger droplets shed most of their mass in the hot combustion products. The theory was that the smaller droplets would form steam in the reaction zone, and the steam in turn would act as an inhibitor, and lower the flame speed. The advanced model would have to be able to emulate the physics involved in the dilution process to correctly predict the variation in flame speed as we use small quantities of inerts in the computation. When we compare with experimental results from chapter three, it is clear that the RUN-1DL evaporation model can not emulate the correct physics.

To consider the effect of increasing water species concentration in the reaction zone, we can look at the change in flame speed for an increasing water vapour concentration. This is shown in Figure 4.21.
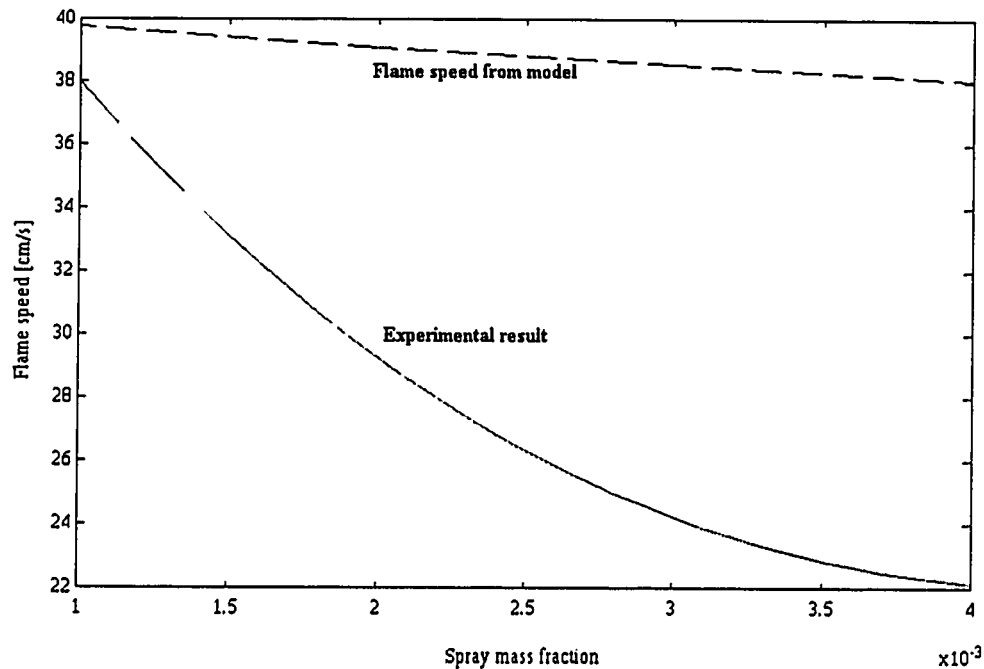
Figure 4.21: Variation in flame speed for increasing water vapour concentration in the reaction zone

The experimental curve in Figure 4.21 comes from Figure 3.7. The model curve was computed by finding the equilibrium state of the reaction system using STANJAN [57]. The equilibrium adiabatic flame temperature was then correlated with velocity data from Figure 4.20.

The model curve represents the expected flame speed due only to cooling of the flame by the water droplets. It is clear from Figure 4.21, that the cooling effect alone does not reduce the flame speed to the same degree as the experiments.

The only viable process that remains is the dilution of the reactants resulting in lower chemical reaction rates in the reaction zone. Lower reaction rates lead to lower flame temperatures and a corresponding reduction in flame speed.

An increase in flame speed after the initial decrease was observed experimentally. The vapour dilution alone was not enough to bring on extinction, and as we increase the water vapour concentration, the flame speed increases. This can be explained by reduced evaporation rates of the individual droplets, as discussed in section 4.2. Reduced droplet evaporation rates means that the droplets no longer evaporate where they are the most useful from a dilution perspective. Instead the individual droplet lifetimes increase, and the droplets shed most of their mass in the combustion products, where their effect is minimal. To bring on extinction we would then need to drastically increase the water droplet concentration in the flame to cool the flame enough to bring on extinction. This brings us to the second mechanism of extinction, which is cooling of the flame until combustion can not be sustained.

Figures 4.22 and 4.23 show the effect of increasing liquid water concentration on adiabatic flame temperature and [OH] concentration. The calculations are equilibrium calculations using STANJAN. The water droplets were introduced into the reactants as equivalent liquid water mass.
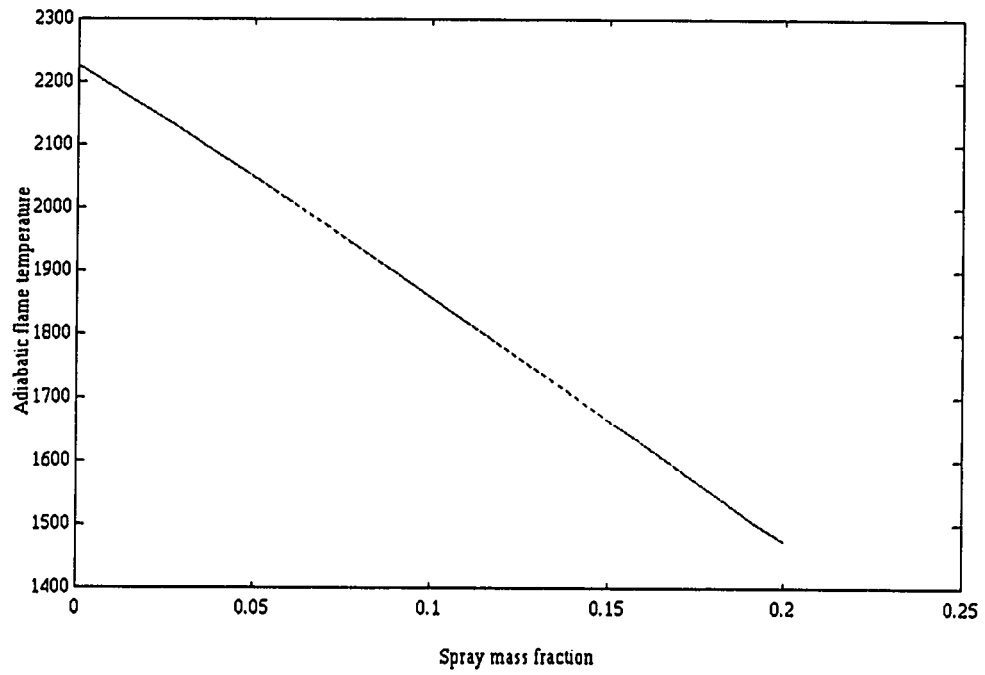
Figure 4.22: Adiabatic flame temperature
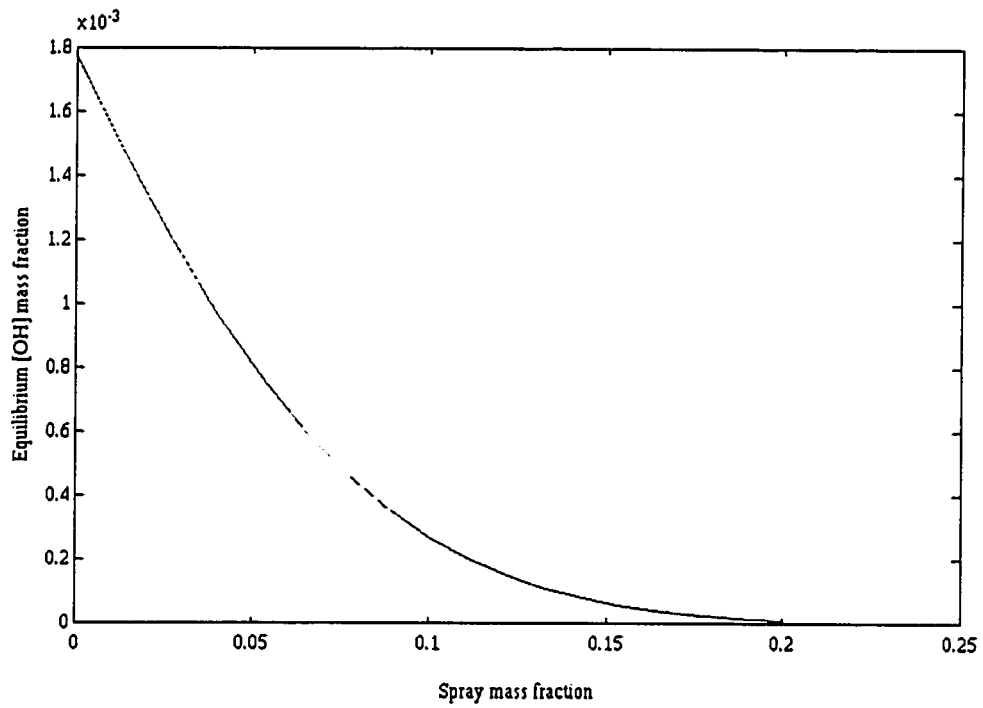
Figure 4.23: [OH] concentration

78

We can see that the extinction point is situated at approximately 1500 Kelvin, where the [OH] concentration levels off to zero. This would mean a mole fraction concentration of 25 percent water in the reactants. This is very close to the experimentally observed value of 26 percent [42].

5. SPRAY GENERATION

This chapter describes two related techniques for generating dense fine sprays of water. The first is a high pressure mixing method involving carbon dioxide and water, and the second is based on the solubility of carbon dioxide in water at elevated pressures.

5.1 Apparatus

5.1.1 High pressure pumping equipment

Figure 5.1 shows a schematic of the high pressure positive displacement pump used for compressing liquids and gases.
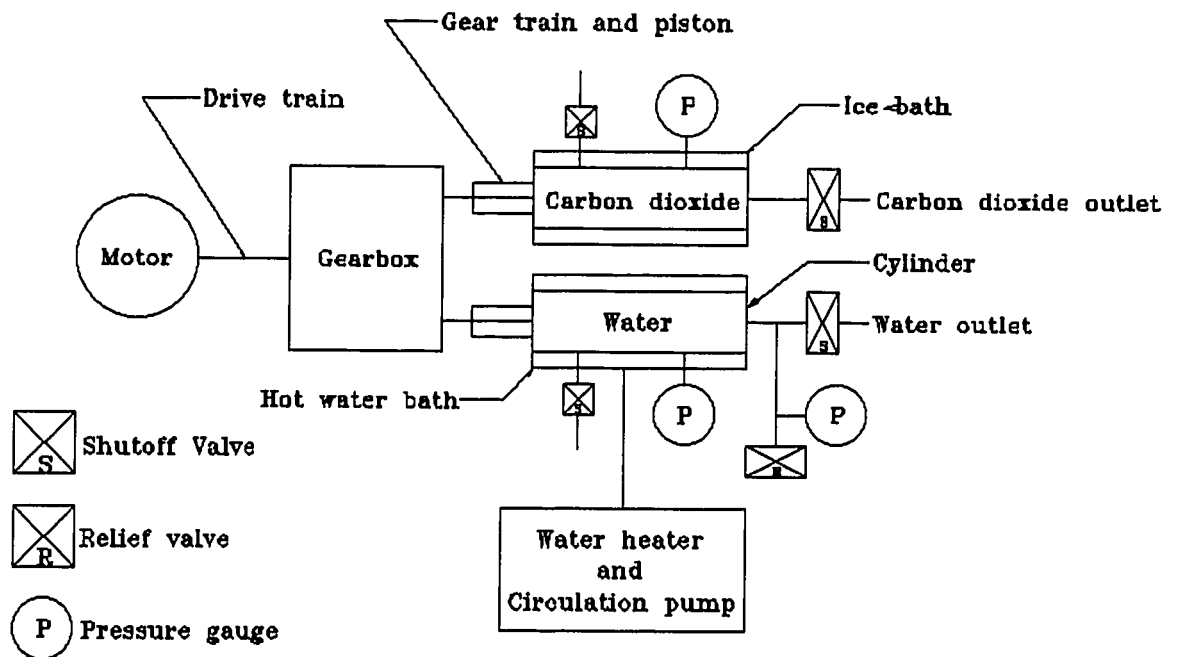
Figure 5.1: High pressure pump schematic

Water and liquid carbon dioxide are contained in two separate cylinders. The water is tap water fed into one cylinder by gravity feed until all air pockets in the cylinder have been eliminated. A shut off valve is then actuated to close off the cylinder to outside air pressure.

Liquid carbon dioxide is drained from a high pressure carbon dioxide tank through a dip tube and piped into the second cylinder. The multiphase mixture of gas and liquid carbon dioxide is cooled in the cylinder by applying a cooling jacket of solid carbon dioxide pellets, going through sublimation at -56 °C, until a homogenous fluid of liquid carbon dioxide exists inside the cylinder. The cylinder is then purged of air pockets by pressurising

the liquid and opening a relief valve until a spray of liquid carbon dioxide emerges.

To pressurise a cylinder, a stainless steel piston is inserted into the cylinder, reducing the space available for the liquid. Pressure integrity for the cylinder is maintained by a high pressure seal at the rear of the cylinder, where the piston is inserted. This arrangement allows for better performance of the seal by eliminating contact between the piston and the walls of the cylinder.

To track the advancement of the piston, and conversely the volume of liquid expelled, the piston is connected to an external pointer and linear scale. The scale is calibrated to cubic centimeters ranging from 0 to 500 units per cylinder. The calibration was confirmed by using a laboratory flask and drawing 10, 50 and 100 cubic centimeters of liquid.

In automatic feed mode both pistons are interlocked by a gearing mechanism, and are not allowed to move independently. Depending on the gear ratio set by a step variable gear box, various flow rates could be obtained. There are 4 ranges (A through D) available, each with seven possible settings within the range. See Table 5.1 for available pump settings.

Gear settings	1	2	3	4	5	6	7
A	5	6.25	7.5	10	12.5	15	17.5
B	20	25	30	40	50	60	70
C	80	100	120	160	200	240	280
D	320	400	480	640	800	960	1120

Table 5.1: Discharge rates in cc/hour per cylinder

To calibrate the flow rate, a laboratory flask was used to draw 10, 50 and 100 cubic centimeters of fluid, and the time required to draw the fluid was measured with a digital stopwatch.

By using a high gear ratio and an electric three phase motor running at constant speed, it was found that any variation in fluid volume output due to pressure loading in the system was negligible.

The mixing arrangement for bringing water and carbon dioxide together at high pressures, is shown in Figure 5.2.
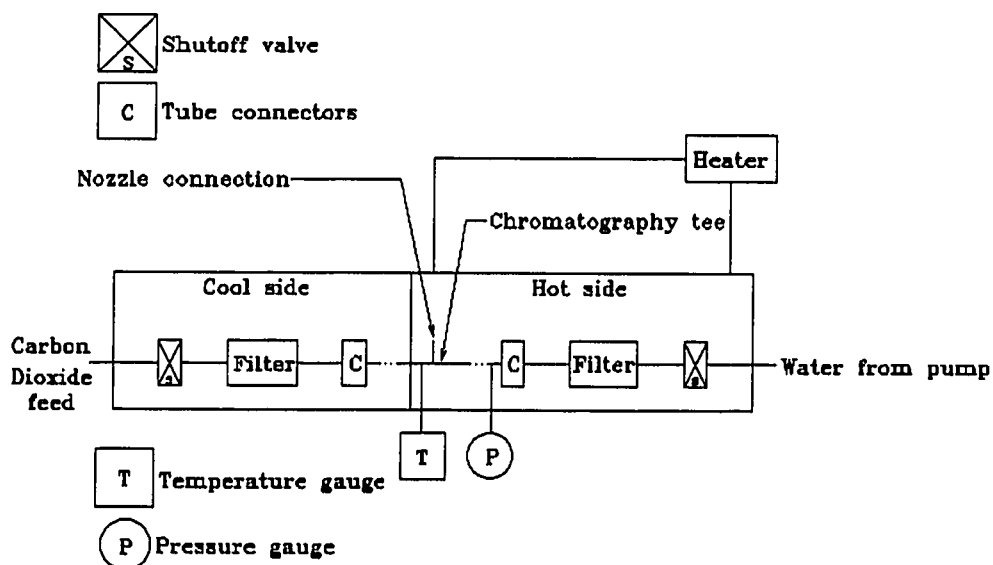
Figure 5.2: Fluid filters, piping and mixing tee.

The mixing section is divided into hot and cool compartments. The cool side is used to maintain the carbon dioxide as a liquid. A liquid phase of carbon dioxide is required at the mixing tee to ensure proper mixing with the water. The hot side is used to heat the water so that the temperature at the mixing tee can be varied. More details on the entire experimental setup are given later.

To ensure purity of the liquids both are pumped through a high capacity filter with an upper cutoff limit of five μm. The output of the filters are connected to a three way chromatography tee. The chromatography tee has a dead volume of only 4×10^{-6} cm^3 . A small mixing volume is absolutely necessary to obtain a spray. Initial experiments were conducted with a mixing tee made from 1/32 inch stainless steel tubing, with an estimated dead volume of

$3x10^{-4}$ cm^3. These experiments resulted in a carbonated water jet issuing from the nozzle, and no spray would form under any conditions. Through a private communication with Professor R.E. Sievers at the University of Colorado at Boulder, the inventor of this spraying technology, it was revealed that to obtain rapid mixing and decompression of the supercritical fluid, a small dead volume mixing tee is required.

The third connection on the chromatography tee has a very fine nozzle attachment. Figure 5.3 shows a more detailed view of the mixing tee and nozzle.
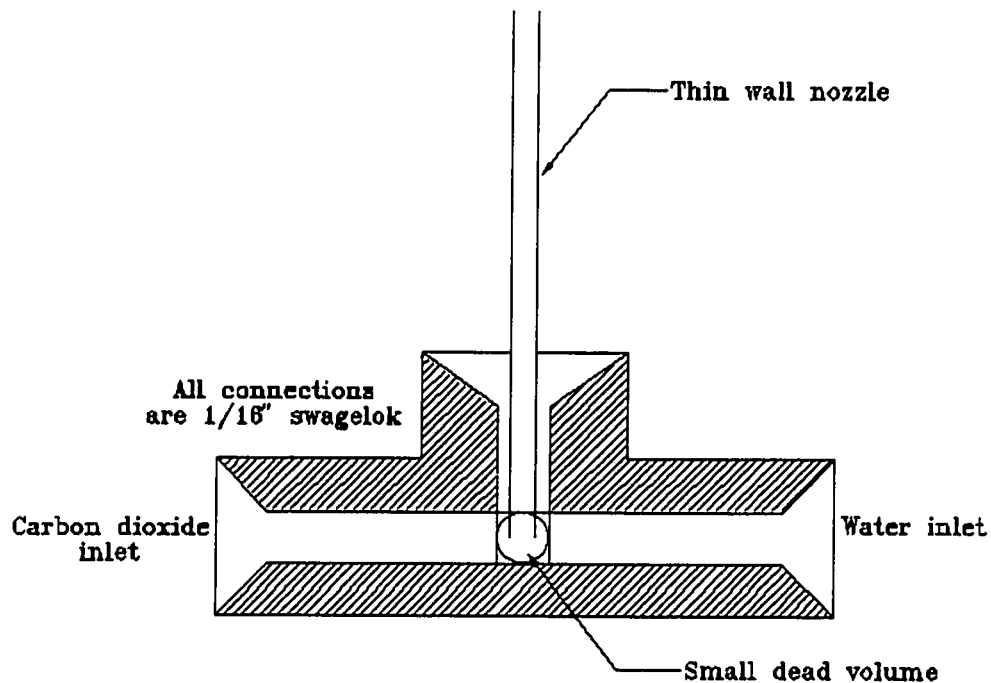
Figure 5.3: Mixing tee and nozzle

The nozzle is custom made with varying length and diameter. Table 5.2 lists the nozzles used in this research.

Nozzle number	Length [cm]	Inside diameter [μm]
1	2.5	63
2	5	63
3	5	100
4	10	100

Table 5.2: Nozzle configurations

The nozzle is a composite design consisting of decreasing sizes of concentric circular tubes. Figure 5.4 shows a typical cross section of the nozzle design.

All dimensions are gauge except otherwise noted
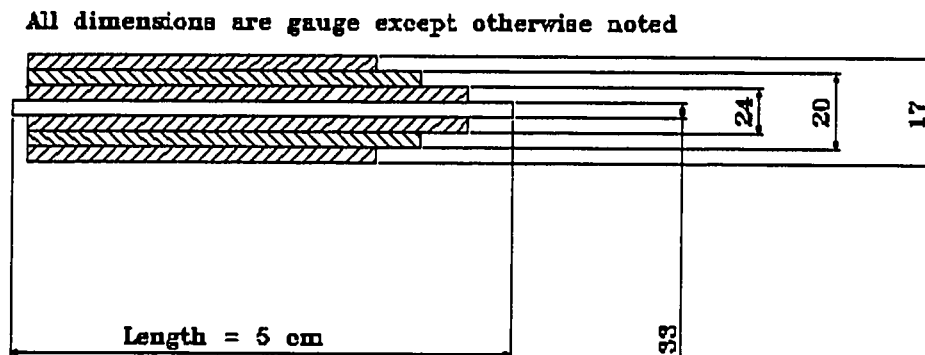
Figure 5.4: Nozzle design

The nozzle is manufactured using high tensile glue to bond and seal the tubes together. It was found that in order to fill in the annular space between the tubes and to maximize the contact area several types of glue were required. The glues used were the Loctite super bonder series, numbers 420, 495 and 496. The super bonder 420 works through capillary action to fill gaps up to 2/1000

of an inch. The 495 is a general adhesive that fills gaps to 4/1000 of an inch, and the 496 was used to bond the outer tube to the nozzle core.

Since the surface area of each tube is used to maximize contact area, the shear forces resulting from applying fluid pressure are equally distributed among the layers, and the high strength adhesives have proven to be a fast and easy way to maintain pressure integrity.

The center tube is the most difficult one to manufacture. Since the inner diameter is only 63 μm and the tube has a very limited wall thickness, any mechanical means of cutting will result in crimping the end of the tube shut and fracturing the tube wall longitudinally. This was observed through a microscope studying the effects of mechanical cutting methods on the smaller tubes. Instead the tube is cut with a 25,000 rpm grinding wheel. This method will result in partial crimping of the tube wall, but will not cause any fractures. The end of the tube is then cut with the acid *aqua regia*. This process will result in the tip of the tube dissolving, and any obstructions inside the tube being cleared. Acid residues are then cleaned off in an ultrasonic cleaner.

The mixing section in Figure 5.2 and the pump in Figure 5.1 are connected by high pressure flexible hoses, to allow for greater movement of the nozzle for measurement purposes. Figure 5.5 shows the complete experimental setup except for diagnostic equipment.
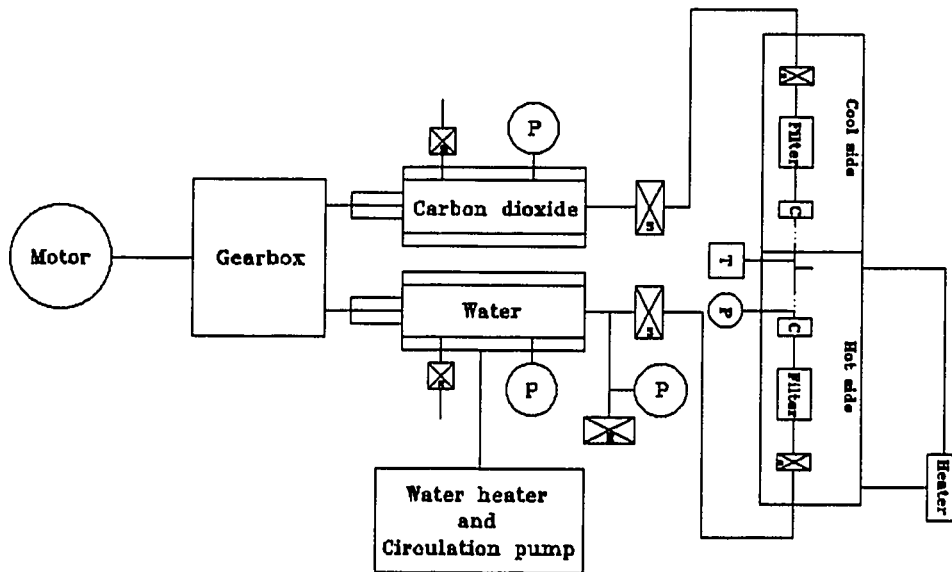
Figure 5.5: Experimental setup

As manufactured, the pump displaces both cylinders at the same rate, resulting in a 50/50 carbon dioxide and water mix, by volume. The design of the pump was altered by placing a secondary gearbox in the carbon dioxide piston feed module.

The flowrate of the two cylinders remain proportional to each other due to the mechanical feed constraints imposed, but now various mixtures of water and liquid carbon dioxide could be achieved. Figure 5.6 shows the possible settings.
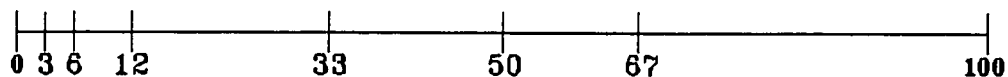
Figure 5.6: Mixture ratios expressed as percent CO_2 by volume

The mixing section shown in Figure 5.2 has a warm and a cool side. The warm side is the nozzle side, and this section is attached to a heating system with a circulation pump. To heat the circulating fluid, the system has a heating coil with two way control, and a temperature feedback from the base of the mixing tee by way of a thermocouple attachment. The setpoint for the heating system could be varied between 25 and 60 degrees Celsius.

The cool side is needed to maintain the carbon dioxide as a liquid. We need to maintain system pressure and incompressibility, and eliminate fluid feed disturbances as a result of changing mixture densities in the carbon dioxide feed line. The only way to accomplish incompressibility is to keep the carbon dioxide in a liquid phase. Figure 5.7 shows the boundary between liquid and gas for carbon dioxide. The dividing line between a supercritical and a subcritical fluid is also shown on Figure 5.7. This is for illustration purposes only, since the carbon dioxide feed line temperature is never allowed to exceed 30 degrees Celsius.
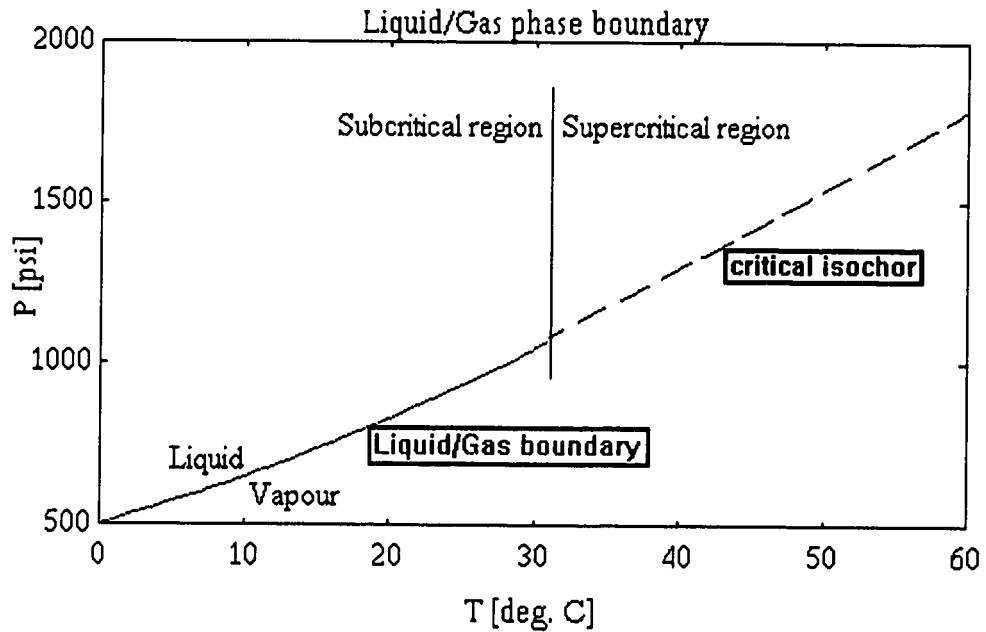
Figure 5.7: Liquid/Gas boundary for carbon dioxide

5.1.2 Pressurized liquid equipment

This section describes an alternate method for producing a fine spray from a carbon dioxide and water mixture. While the previous approach is complex and involves a considerable amount of equipment, this method is very simple. The trade off in using a single pressurised cylinder is that the amount of carbon dioxide in the mixture is now fixed.

Figure 5.8 shows the high pressure cylinder used in the approach where carbon dioxide is dissolved to its solubility limit in water.
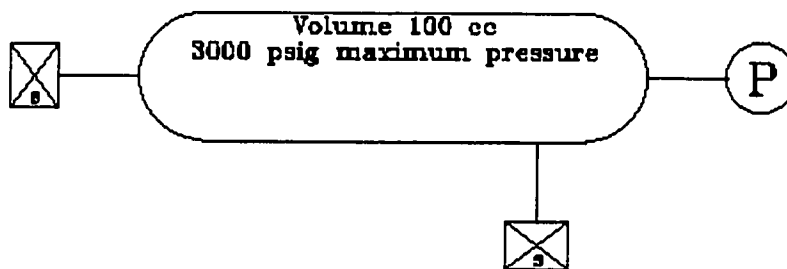
Figure 5.8: High pressure mixing cylinder with connections

The pressure cylinder has a dead volume of 100 cubic centimeters, and is certified to 3000 psi of pressure. It has two connections with shut off valves attached. The cylinder is filled with tap water using the bottom valve to displace any air inside the cylinder. The top valve is then closed and the cylinder is pressurised by injecting water from a positive displacement pump, until the desired pressure is achieved.

The cylinder is then disconnected from the water source, and reconnected to a variable pressure liquid carbon dioxide source. The carbon dioxide liquid pressure is adjusted to match the cylinder pressure and the shutoff valve to the cylinder is opened. The system pressure can now be set by changing the pressure of the carbon dioxide source.

The second valve at the opposite end of the cylinder is opened, and a specified amount of water is withdrawn from the cylinder while maintaining constant system pressure injecting carbon dioxide. There is now a mixture of water and liquid carbon

dioxide inside the cylinder. The liquid carbon dioxide shutoff valve is closed and the cylinder is allowed to come to equilibrium. This will result in a pressure drop as the carbon dioxide dissolves into the water, to the amount determined by the solubility limit.

When the cylinder has come to an equilibrium state it is once again connected to the carbon dioxide pressure source, and the system pressure is increased by injecting liquid carbon dioxide until the desired pressure is reached.

To enhance mixing of the liquid carbon dioxide and water, the cylinder is tilted 45 degrees back and forth several times during the mixing cycle. The whole process takes three days to accomplish, during which time the surrounding temperature of the cylinder is kept fairly constant by keeping the cylinder submerged in a temperature control water bath. Maintaining a constant cylinder temperature is important, since the solubility limit of carbon dioxide in water is strongly dependent on temperature.

When one of the nozzles from table 5.2 is attached to the cylinder and the shutoff valve is opened, a dense fine spray will form at the nozzle exit.

The flowrate of the spray was determined by spraying the fluid into a laboratory flask and recording the time to achieve 5, 10 and 20 cubic centimeters. The flowrate was fairly constant due to the expansion of liquid carbon dioxide coming out of solution as the pressure decreased inside the cylinder.

5.2 Diagnostics

5.2.1 Quality measurements

To determine the quality of the spray, i.e. the size distribution of the droplets, two different types of equipment were used. The first was a phase doppler anemometry system and the second was a time of flight system.

5.2.1.1 Phase doppler anemometry

The phase doppler works on the principle of light scattering. By analyzing the frequency spectrum of reflected and refracted light from a particle being illuminated by a laser light source, the size and velocity of a particle can be determined.

To calibrate the phase doppler, dried particles of polystyrene were used. The polystyrene particles were 1, 5 and 10 μm in size. The particles were aerosolized by using a medical nebulizer and spraying a solution of particles in water into a drying chamber that consisted of a large Plexiglas tube with air flow entering perpendicular to the nebulizer spray direction. The particles were measured by the phase doppler system and it was found that the distribution was monotonic with a size deviation of no more than five percent from the stated mean.

When measuring the nozzle sprays the measurement point in the spray cone was one centimeter up from the tip of the nozzle and in the lateral plane visually determined as the center of the spray.

The phase doppler anemometer used for this study was the Dantec model 58N10 configured for one-dimensional measurements using three photodetectors.

5.2.1.2 Time of flight instrument

Time of flight methods to determine particle size is based on the simple concept of particle drag. The flow that the particle resides in is accelerated from a low velocity to near sonic velocity. The inertia of the particles results in different rates of acceleration for different sizes of particles. The size of the particle can be determined by measuring the time of flight between two laser beams. Heavier particles will have a longer flight time than lighter particles thereby creating a correlation between size and time of flight.

Like the phase doppler system, the calibration specimens were dried polystyrene particles of sizes 1, 5 and 10 micrometer.

Aerodynamic time of flight methods will measure a size distribution, but the particle velocities can not be determined with this instrument. A time of flight system is therefore limited in its scope of use.

To use this diagnostic method the particles must first be collected and sampled in a well controlled flow. This was done by having the experimental apparatus spray droplets into a large closed vessel. Once the vessel was saturated with droplets, the time of flight instrument would draw a sample from the vessel at a fixed flow rate.

The time of flight instrument used in this study was the Aerosizer Mach 2 by Amherst Process Instruments Inc.

5.2.2 Comparing the phase doppler to the time of flight instrument

The calibration data was compared between the phase doppler and the time of flight instrument. It was found that for smaller particles, there was a negligible difference in reported data. However, as the particles increased in size there was a difference of about 20 percent. As the data from the nozzles were compared, this difference increased to 30 percent. This is most likely due to the difficulty in getting a representative sample from the spray. Larger particles were more difficult to capture with the time of flight instrument, and this data would consistently indicate count, surface and mass mean values that were lower than those measured with the phase doppler system. It was therefore decided to use the phase doppler as the primary tool for gathering spray data, and to use the time of flight instrument for independent comparison of trends in

the measurements. The time of flight instrument was also used for sampling the whole spray, since the phase doppler only gives a point measurement. However, due to the severe biasing of spraying droplets into a vessel and sampling from that vessel, the time of flight data collected in this fashion was not used further in this study.

5.3 Results

5.3.1 High pressure pumping apparatus

Table 5.3 shows the results of an experiment with nozzle number four, nozzle diameter is 100 μm and nozzle length is 10 centimeters.

All diameters measured are in μm, the pressures are pounds per square inch - gauge, and the temperature was measured in degrees Celsius. Two data points for 25 °C, 1000 and 1100 psig pressure always resulted in an oscillatory spray output between a jet and a spray. The behaviour observed most frequently was the jet, and the droplet sizes from the jet breakup are therefore recorded in Table 5.3 with the label (Jet). The mixture ratio of carbon dioxide and water was 50/50, i.e. always above the solubility limit for carbon dioxide in water.

Pressure [psig]	900	1000	1100	1200	1300
Temperature 25 °C					
D10	5.92	8.33 (Jet)	7.32 (Jet)	4.74	4.45
D30	7.94	12.62(Jet)	10.19(Jet)	6.17	5.60
Temperature 30 °C					
D10	5.95	5.71	5.04	4.70	4.57
D30	7.94	7.67	6.64	6.13	5.79
Temperature 35 °C					
D10	4.81	5.77	5.25	4.78	4.57
D30	6.04	7.72	6.88	6.15	5.88
Temperature 40 °C					
D10	4.87	5.40	5.70	5.53	4.69
D30	6.33	7.16	7.23	7.05	5.92

Table 5.3: Droplet sizes, D10 is count mean diameter, D30 is mass mean diameter. D10 and D30 are defined on page 98. The droplet size measurements are accurate to within one percent.

$$D_{10} = \frac{\sum\limits_{i=1}^{N} D_i}{N} \qquad D_{30} = \left(\frac{\sum\limits_{i=1}^{N} D_i^3}{N} \right)^{1/3}$$

D_i = droplet diameters

N = number of droplets

Figure 5.9 shows the variation of count and mass mean diameter with changing nozzle geometry, for a pressure of 1300 psig, and a temperature of 35 degrees Celsius.
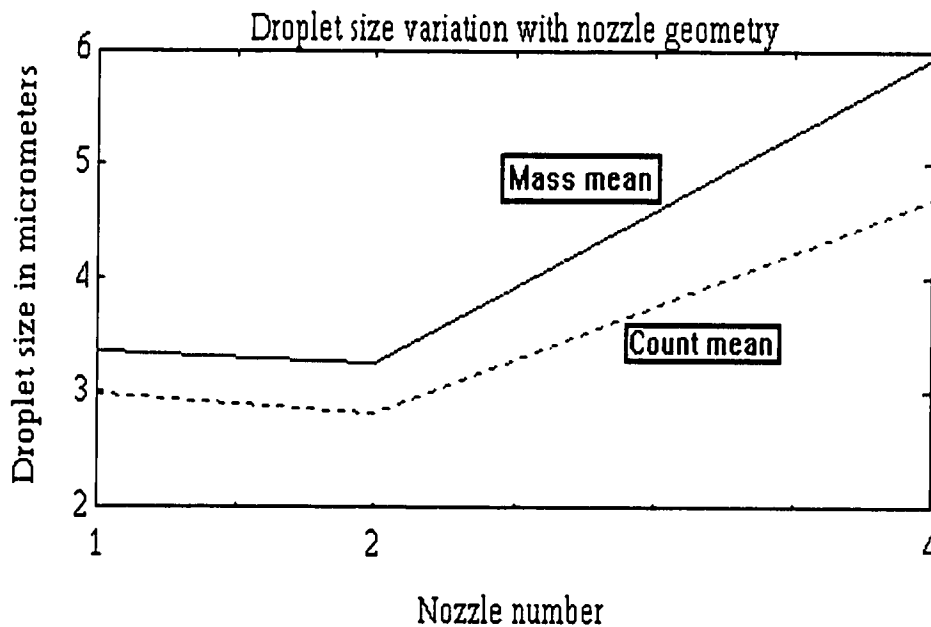
Figure 5.9: Count and mass mean diameter versus nozzle geometry

Looking at the data points in Table 5.3 near the critical point for carbon dioxide ($P_{crit} = 72$ atm., and $T_{crit} = 31.3$ °C), we can see that in this region the droplet sizes decrease with increasing pressure and increase with increasing temperature. To understand this phenomenon we need to look at the phase diagram for carbon dioxide. Figure 5.10 shows a phase diagram for carbon dioxide, adopted from Din [46].

Figure 5.10: Simplified temperature versus entropy diagram

Below the critical temperature, as we increase the pressure the solubility of carbon dioxide in water increases monotonically.

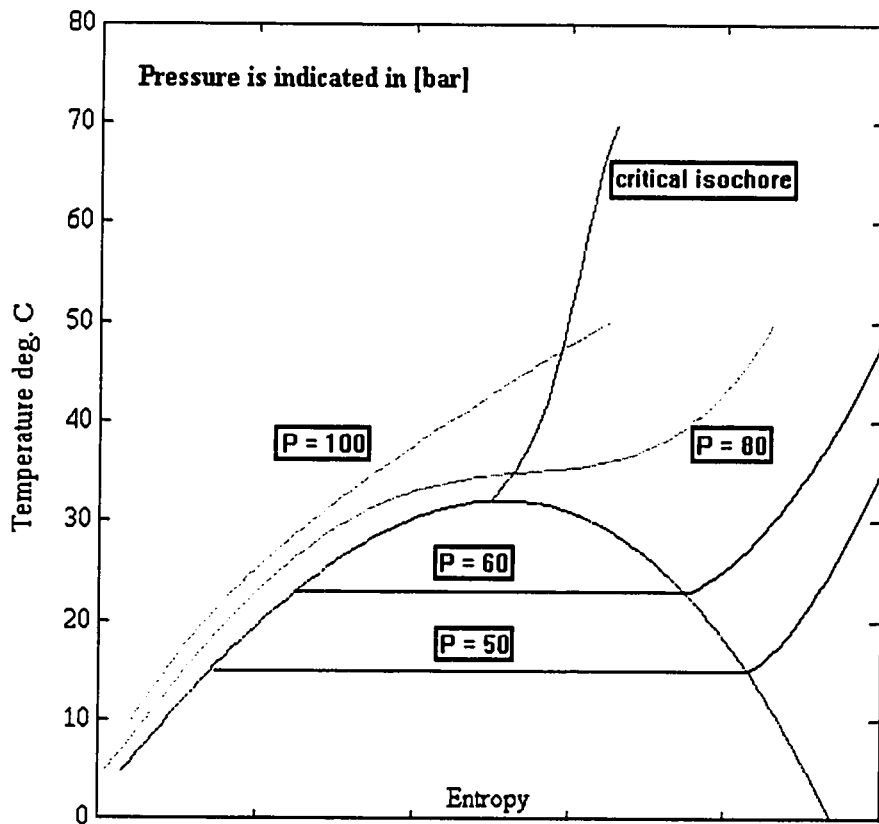Table 5.4 is a minimized adaptation of data from Wiebe and Gaddy [33], on the solubility of carbon dioxide in water at various temperatures from 12 to 40 degrees Celsius.

Pressure [atm]	T = 25 °C	T = 31 °C	T = 35 °C	T = 40 °C
50	27.2	24.1	22.2	20.3
75	31.1	29.3	27.8	25.8
100	31.7	30.1	29.1	27.8

Table 5.4: Solubility cc. S.T.P. per gram of water

Arguing that increasing solubility of carbon dioxide in water will give smaller droplet sizes is correct based on the droplet size data for 30 degrees Celsius. However, when we look at the droplet size data for 35 and 40 degrees Celsius from Table 5.3, which is above the critical temperature for carbon dioxide, we see that the droplet sizes actually increase initially with increasing pressure, even though the solubility of carbon dioxide in water is rising.

This phenomena can be explained by looking at Figure 5.10, and introducing the critical isochore as a dividing line between two regions of droplet creation. On the left side of the critical isochore we have pressurised liquid, and on the right side we have superheated vapor. Referring to Altunin and Vukalovich [45], page 72, "... a liquid/vapor phase transition involving a structural change also occurs in the supercritical region. However, in contrast to the

subcritical region, this transition is continuous and microheterogeneous in form.". The authors go on to state that "... the critical isotherm cannot be considered as the boundary between the liquid and vapor ...".

Following this argument means that as we are about to cross the critical isochore we have a multiphase mixture of liquid and gaseous carbon dioxide and water. This multiphase mixture changes properties in a continuous and microheterogeneous way, and we have the possible situation of dealing with continuously changing mixing conditions. This contributes to an instability in the droplet creation process, and the conclusion is that this area should be avoided for droplet production.

Vukalovich and Altunin [45] also define the transition boundary as the area "... between the lines of maxima of the derivative dv/dT at constant pressure and the maxima of the specific heat C_p along the isobars ...". This definition has the effect of expanding an area around the critical isochore, in which the formation of a steady spray is impossible.

Analysing the data for different nozzle geometries, we find that there is no real difference between nozzles one, two and four as shown in Figure 5.9. The fourth nozzle produces slightly larger droplets, the difference being 1.5 μm in count mean diameter average, and this is likely due to variances in the phase doppler measurement setup. Changing the needle length does not affect droplet production at all.

5.3.2 Solubility apparatus

To confirm that the dominating effect on droplet size is solubility, the pressurized cylinder described in chapter 5.1.2 was attached to all four nozzles, and the spray was measured using the phase doppler anemometer. The result was a spray with mass mean diameter equal to 10 μm, and it was found that the droplet size was independent of cylinder pressure, temperature, and nozzle geometry. This only leaves the amount of carbon dioxide injected into the cylinder as the remaining factor.

To confirm the effects of varying concentrations of carbon dioxide, the high pressure pump was run at all the settings shown in Figure 5.7. When the amount of carbon dioxide in the water was reduced below the saturation limit, no spray could be obtained, and instead a carbonated water jet was obtained. Conversely, when the amount of carbon dioxide was increased above the solubility limit, a spray readily formed.

6. CONCLUSIONS

A study of the process of flame suppression by fine water mists has been conducted. It was found that there are two possible mechanisms for reducing the propagation speed of a laminar, premixed methane and air flame.

The first process is the dilution of the reacting species by introducing an inert such as water vapour. The water vapour comes from evaporating droplets that are smaller than five μm in size. It was shown by numerical modelling of droplet evaporation in a temperature and velocity field from a stoichiometric flame that droplets smaller than five μm in diameter evaporate completely in the preheat and reaction zones. This was considered to be a requirement for effective dilution of the fuel and oxidizer species.

The second process is heat extraction from the flame. It was shown that heat extraction is not important in the initial stages of flame suppression. However, as the droplet loading increased, heat extracted from the flame resulted in a reduction in flame speed.

It was further shown that the two processes of suppression work at different times in the evolution of a flame subjected to a fine water mist. Vapour dilution reduces the flame speed significantly at low droplet loadings. At high droplet loadings, heat extracted from the flame is the major factor in reducing flame speed.

In the transition region between low and high droplet loadings, the flame speed increases before enough water mass can be injected into the system to bring it into the high droplet loading regime.

The flamelet code RUN-1DL in its present configuration can not be used to elucidate the effects of dilution in the reaction zone. The modelling consists of the droplet and flame interaction behaving as a simple "heat in - mass out" model, with the appropriate damping terms in the droplet equations to control the evaporation rate. However, the flamelet code was useful for obtaining numerical data on flame propagation speeds, and to evaluate the simple droplet evaporation model.

The work on generating water sprays resulted in a useful apparatus for producing very fine mists. The results from the spray generation studies indicate that for the technology to work there is no need to obtain a supercritical thermodynamic state. The spray formation is closely related to the solubility limit, and hence the amount of carbon dioxide available in the mixture.

7. FUTURE WORK

The data on flame behaviour is incomplete. The range of water spray concentration can be expanded with the help of the spray generation apparatus. The rich flames became buoyantly unstable for low concentrations of water spray. Even though the behaviour of the rich flames at low concentrations can be inferred from the data, there is a need to collect flame speed data for the rich flames. A method has to be devised to stabilize the rich flames so that flame speed measurements can be made.

The modelling of flame behaviour is in the early stages. The current computer code (RUN-1DL) has a problem converging to a solution when the water droplet concentration is raised above a critical value. The flame behaviour predicted by the flamelet model is inconsistent with the experimental data for low water droplet concentrations. A new model for flame and droplet interaction has to be developed.

The theory of droplet formation for supercritical fluids is incomplete. A thermodynamic model needs to be created to explain the phenomena of fine droplet generation. Additional measurements at high levels of supercritical solvent needs to be made to map out the entire range of solvent mass fractions.

A flame suppression system needs to be designed and tested from an engineering perspective to verify the practical application of a flame suppression system utilising fine water mists. An example of how this system may be designed is given in Figure 7.1.
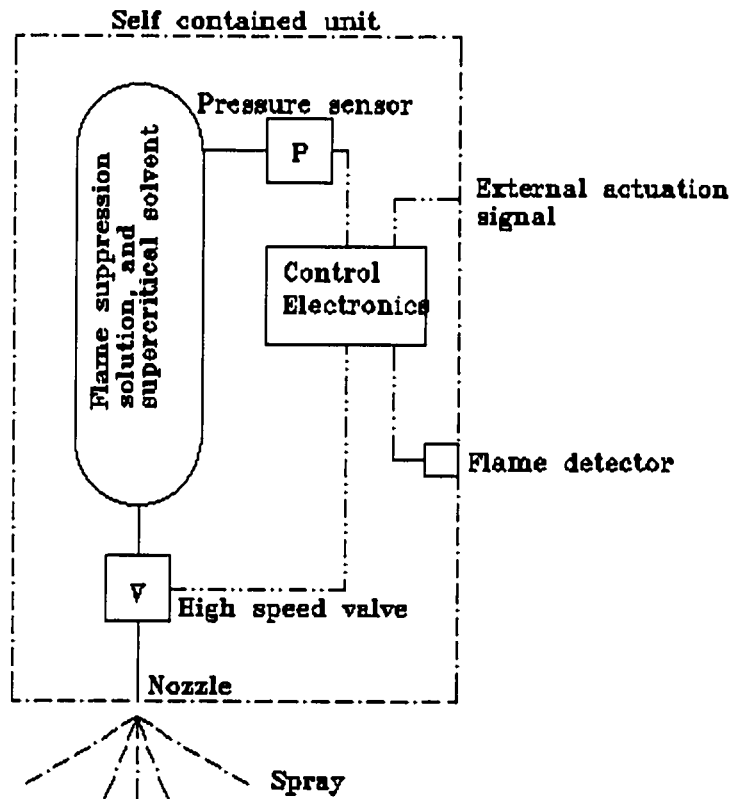

Figure 7.1: Flame suppression system using fine water mists

To generate the fine sprays required for flame suppression in the lab, a modified version of the flame suppression system in Figure 7.1. can be used. This system would use the pressurised cylinder filled with extingushing medium and supercritical solvent, but exclude the flame detection and spray actuation components.

A spray generation system that does not use the high pressure pump to mix the fluids would be much easier to operate. It would also yield more consistent results since the desired spray properties can be set before starting the flame experiments.

REFERENCES

[1] Coward H.F., Gleadall J.J. "Extinction of Methane Flames by Water Vapor" J. Chem. Soc., 1930, p.243

[2] Yeaw, J.S., Shnidman L, "The extinction of Gas Flames by Steam" AGA Proc., 1938, p.717

[3] Braidech M., Neale J.A., "The Mechanism of Extinguishment of Fire by Finely Divided Water", The National Board of Fire Underwriters, New York, 1955

[4] Rasbash D.J., Rogowski Z.W., Stark G.W.V., "Mechanisms of Extinction if Liquid Fires with Water Sprays", Combustion and Flame, 1960, vol.4, pp.223-234

[5] Rasbash D.J., Rogowski Z.W., "Extinction of Fires in Liquids by Cooling with Water Sprays", Combustion and Flame, 1957, vol.1, pp.453-466

[6] Sapko M.J., Furno A.L., Kuchta J.M., "Quenching Methane-Air Ignitions With Water Sprays", Report of Investigations 8214, Bureau of Mines, United States Department of the Interior, 1977

[7] Ng D., Sapko M., Furno A., Pro R., "Coal Dust and Gas Explosion Suppression by Barriers", Industrial Dust Explosions, ASTM STP 958, Kenneth L. Cashdollar and Mertin Herzberg, Eds., American Society for Testing and Materials, Philadelphia, 1987, pp.138-151

[8] Zhou D.B., Lu Z.J., "Research on the Suppression of Coal Dust Explosions by Water Barriers", Industrial Dust Explosions, ASTM STP 958, Kenneth L. Cashdollar and Mertin Herzberg, Eds., American Society for Testing and Materials, Philadelphia, 1987, pp.152-157

[9] Thomas G.O., Jones A., "The Mitigation of small scale Hydrocarbon-Air Explosions by Water Sprays", Trans. IChemE, vol.70, Part A, March 1992

[10] Thomas G.O., Brenton J.R., Al-Hassan T., "On the controlling parameters during explosion mitigation by water sprays", Paper presented at the ERA Conference on Offshore Safety and Structural Design, London, November 1994

[11] Thomas G.O., Brenton J.R., Al-Hassan T., "Small Scale Studies of Water Spray Dynamics During Explosion Mitigation Tests", Paper from proceedings IChemE, Advances in Process Safety, UMIST Manchester, April 1994

[12] Thomas G.O., Edwards M.J., Edwards D.H., "Studies of Detonation Quenching by Water Sprays", Combustion Science and Technology, vol.71, 1990, pp.233-245

[13] Thomas G.O., Jones A., Edwards M.J., "Influence of Water Sprays on Explosion Development in Fuel-Air Mixtures", Combustion Science and Technology, May, 1991

[14] McCaffrey B.J., "Jet Diffusion Flame Suppression using Water Sprays - An Interim Report", Combustion Science and Technology, vol.40, 1984, pp.107-136

[15] Watts J.W., "Effects of Water Spray on Unconfined Flammable Gas", Loss Prevention, 10, 1976, pp.48-54

[16] Mawhinney J.R., Dlugogorski B.Z., Kim A.K., "A closer look at the fire extinguishing properties of water mist", The International Association for Fire Safety Symposium, Ottawa, June, 1994

[17] Schoen W., Droste B., "Investigations of water spraying systems for LPG storage tanks by full scale fire tests", Journal of Hazardous Materials, 20, 1988, pp.73-82

[18] Chein H., Lundgren D., "A High-Output, Size-Selective Aerosol Generator", Aerosol Science and Technology, 23, 1995, pp. 510-520

[19] Chen B.T., Yeh H.C., Rivero M.A., "Use of two virtual impactors in series as an aerosol generator", Journal of Aerosol Science, vol.19, 1988, pp.137-146

[20] Walton A.W.H., Prewitt W.C., "The production of sprays and mists of unifrom size by means of a spinning disk type sprayer", Proc. Phy. Soc., 9, B62, 1949, pp.341-350

[21] Berglund R.N., Liu B.Y.H., "Generation of monodisperse aerosol standards", Envir. Sci. Technology, 7, 1973, pp.147-153

[22] Mercer T.T., Goddard R.F., Flores R.L., "Output characteristics of three ultrasonic nebulizers", Ann. Allergy, 26, 1968, pp.18-27

[23] Mercer T.T., Goddard R.F., Flores R.L., "Output characteristics of several commercial nebulizers", Ann. Allergy, 23, 1965, pp.314-326

[24] Ellcey, E.C., "Droplet formation and breakup for a prototype swirl injector", M.S. Thesis, Michigan Technological University, 1989

[25] Sievers R.E., private communication, July, 1995

[26] Hybertson B.M., Hansen B.N., Barkley R.M., Sievers R.E., "Deposition of palladium films by a novel supercritical fluid transport-chemical deposition process", Mat. Res. Bull., vol.26, 1991, pp.1127-1133

[27] Sievers et.al, United States Patent number 5,301,664

[28] Hybertson B.M., Hansen B.N., Barkley R.M., Sievers R.E., "Supercritical Fluid Transport - Chemical Deposition of Films", Chemistry of Materials, 4, 1992, pp.749-753

[29] Sievers, et.al., International Patent Number PCT/US88/04519

[30] Johnston K.P., "New directions in supercritical fluid science and technology", chapter one, Supercritical Fluid Science and Technology, 1989

[31] McNally M.E.P., Bright F.V., "Fundamental Studies and Applications of Supercritical Fluids", chapter one, Supercritical Fluid Technology

[32] King M.B., Mubarak A., Kim J.D., Bott T.R., "The Mutual Solubilities of Water with Supercritical and Liquid Carbon Dioxide", The Journal of Supercritical Fluids, 5, 1992, pp.296-302

[33] Wiebe R., Gaddy V.L., "The solubility of Carbon Dioxide in Water at Various Temperatures from 12 to 40° and at Pressures to 500 Atmospheres. Critical Phenomena" Solubility of Carbon Dioxide in Water, April, 1940

[34] Chun B.S., Wilkinson G.T., "Interfacial Tension in High Pressure Carbon Dioxide Mixtures", Proceedings of the 3rd International Symposium on Supercritical Fluids, vol.1, pp.43-51, Oct. 17-19, 1994, Strasbourg, France

[35] Pech D.G., Johnston K.P., "Prediction of Interfacial Properties in Microemulsions: The Lattice Fluid Self-Consistent Field Theory", J. Phys. Chem., 97, 1993, pp.5661-5667

[36] Faeth G.M., Hsiang L.P., Wu P.K., "Structure and breakup properties of Sprays", Int. J. Multiphase Flow, vol.21, 1995, pp.99-127

[37] Rogg B., "RUN-1DL: A Computer Program for the Simulation of One-Dimensional Chemically Reacting Flows", Technical Report CUED/A-THERMO/T39, University of Cambridge, Department of Engineering, April, 1991

[38] Mitani T., Niioka T., "Extinction Phenomenon of Premixed Flames with Alkali Metal Compounds", Combustion and Flame, 55, 1984, pp.13-21

[39] Mitani T., "A Flame Inhibition Theory by Inert Dust and Spray", Combustion and Flame, 43, 1981, pp.243-253

[40] Sermange M., "Contribution to the numerical analysis of laminar stationary flames", Lecture noted in physics, no. 241, pp. 375-388

[41] Chen N.H., Rogg B., Bray K.N.C., "The effect of water on laminar flame structure", Proc. joint meeting of the British and German sections of the Combustion Institute, pp.348-351, Cambridge, UK, March 29 - April 2, 1993

[42] Thomas G.O., "An estimation of the quenching limits for laminar methane-air flames due to water droplet evaporation", private communication, June, 1996

[43] Morel T., "Comprehensive Design of Axisymmetric Wind Tunel Contractions", Journal of Fluids Engineering, June, 1975, pp.225-378

[44] Rogg B., "Response and Flamelet Structure of Stretched Premixed Methane-Air Flames", Combustion and Flame

[45] Vukalovich M.P., Altunin V.V., "Thermophysical Properties of Carbon Dioxide", Collet's Publishing, London, 1968

[46] Din F., "Thermodynamic Functions of Gases", Volume 1, Butterworths Scientific Publications, London, 1956

[47] Cengel Y.A., Boles M.A., "Thermodynamics: an engineering approach", McGraw-Hill, 1994

[48] Lixing Z., "Theory and Numerical Modeling of Turbulent Gas-Particle Flows and Combustion", Science Press and CRC Press, 1993

[49] Bird B.R., Stewart W.E., Lightfoot E.N., "Transport Phenomena", John Wiley & Sons

[50] Kays W.M., Crawford M.E., "Convective Heat and Mass Transfer", McGraw-Hill

[51] Crowe C.T., "Fluid-Particle Flows, Fundamental Concepts and Numerical Models", Syncrude seminar, February 20-21, 1997

[52] Rogg B., "RUN-1DL Users manual", University of Cambridge, report CUED/A-THERMO/TR39

[53] Incropera F.P., Dewitt D.P., "Introduction to Heat Transfer", John Wiley & Sons, 1990

[54] Williams, F.A., "Combustion Theory", The Benjamin / Cummings Publishing Company, 1985

[55] Mawhinney, J.R., "Water-Mist Fire Suppression Systems for the Telecommunication and Utility Industries", NRC-CNRC Fire Research News, Issue No.74, Fall, 1994

[56] Nandakumar K., "Lecture Notes in Computational Methods in Chemical Engineering", Department of Chemical Engineering, University of Alberta, Edmonton, Alberta, Canada

[57] Wm. C. Reynolds, Stanford University, IBM PC shareware

APPENDIX A: ROTAMETER DATA

By constructing tables with a main index of pressure, and further index the tables to the rotameter reading, the flow rate of each gas can be determined, and an equivalence ratio calculated. Table A.1 is the calibration chart for an air pressure of 26 psig, and a fuel pressure of 25 psig.

| Equivalence ratio for air rotameter reading 8.7 units	Fuel rotameter reading [units]
0.5	3.6
0.6	4.0
0.7	4.3
0.8	4.6
0.9	4.9
1.0	5.2
1.1	5.5
1.2	5.8
1.3	6.1
1.4	6.4
1.5	6.7

Table A.1: Rotameter fuel calibration chart

APPENDIX B: METHANE DETECTOR
CALIBRATION PROCEDURE

To calibrate the Methane detector, two bottles of certified gases were purchased. The first calibration gas was methane at a concentration of 50 percent LEL with the balance being dry air. The second calibration gas was 50 percent methane by volume with the balance being Nitrogen.

By flowing the gases through the detector for several minutes at a time, the electrocatalytic pellistor would be saturated with the gas mixture, and the zero would be set for that range. After the instrument was calibrated, it was tested with four different mixtures of gas, all containing varying levels of natural gas. In order they were: dry air with zero percent methane, 50 percent LEL, 50 percent by volume, and 100 percent by volume

IMAGE EVALUATION
TEST TARGET (QA-3)
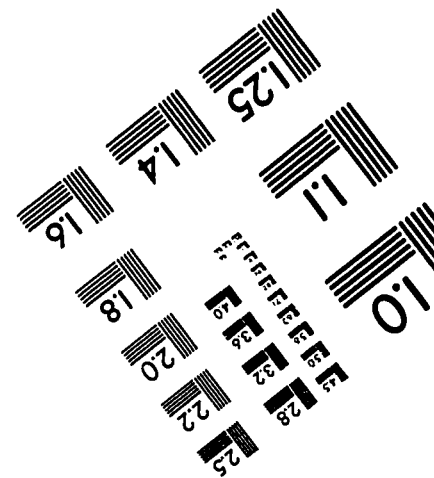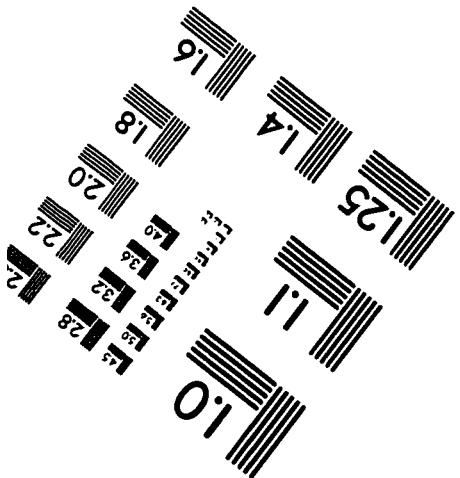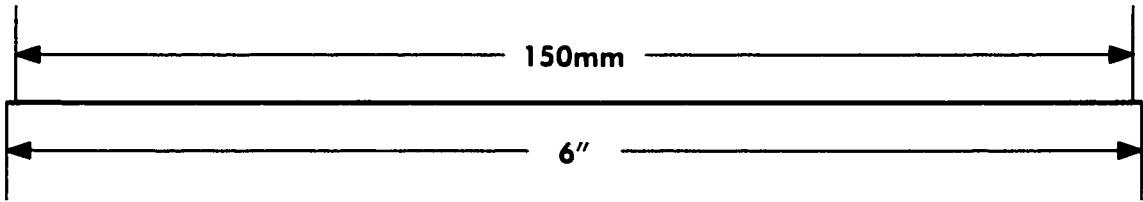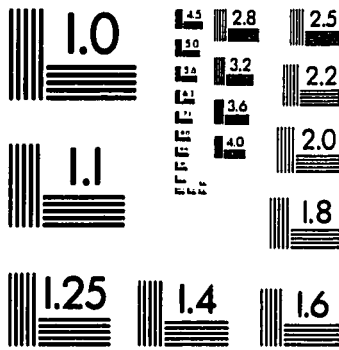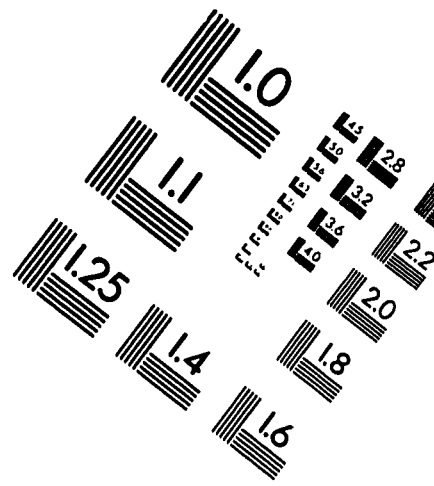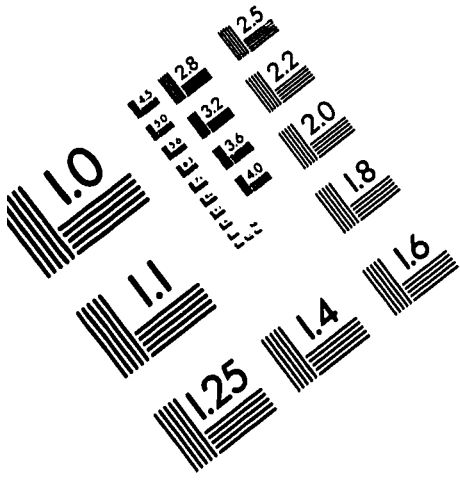
APPLIED IMAGE , Inc
1653 East Main Street
Rochester, NY 14609 USA
Phone: 716/482-0300
Fax: 716/288-5989